energies

MDPI

Article

# Part-Load Energy Performance Assessment of a Pumped Thermal Energy Storage System for an Energy Community

**Emanuele Nadalon [1], Ronelly De Souza [1,2], Melchiorre Casisi [3,*] and Mauro Reini [1]**

[1] Department of Engineering and Architecture, University of Trieste, 34127 Trieste, Italy; emanuele.nadalon@dia.units.it (E.N.); ronellyjose.desouza@phd.units.it (R.D.S.); reini@units.it (M.R.)
[2] GITSE-I3A, Department of Mechanical Engineering, Universidad de Zaragoza, 50018 Zaragoza, Spain
[3] Polytechnic Department of Engineering and Architecture, University of Udine, 33100 Udine, Italy
* Correspondence: melchiorre.casisi@uniud.it

**Abstract:** Research on pumped thermal energy storage (PTES) has gained considerable attention from the scientific community. Its better suitability for specific applications and the increasing need for the development of innovative energy storage technologies are among the main reasons for that interest. The name Carnot Battery (CB) has been used in the literature to refer to PTES systems. The present paper aims to develop an energy analysis of a CB comprising a high-temperature two-stage heat pump (2sHP), an intermediate thermal storage (latent heat), and an organic Rankine cycle (ORC). From a broad perspective, the CB is modeled considering two types of heat inputs for the HP: a cold reservoir in the ground (at a constant temperature of 12 °C throughout the entire year) and a heat storage at 80 °C (thermally-integrated PTES—TI-PTES). The first part defines simple models for the HP and ORC, where only the cycles' efficiencies are considered. On this basis, the storage temperature and the kind of fluids are identified. Then, the expected power-to-power (round-trip) efficiency is calculated, considering a more realistic model, the constant size of the heat exchangers, and the off-design operation of expanders and compressors. The model is simulated using Engineering Equation Solver (EES) software (Academic Professional V10.998-3D) for several working fluids and different temperature levels for the intermediate CB heat storage. The results demonstrate that the scenario based on TI-PTES operation mode (toluene as the HP working fluid) achieved the highest round-trip efficiency of 80.2% at full load and 50.6% round-trip efficiency with the CB operating at part-load (25% of its full load). Furthermore, when the HP working fluid was changed (under the same scenario) to R1336mzz(Z), the round-trip full-load and part-load efficiencies dropped to 72.4% and 46.2%, respectively. The findings of this study provide the HP and ORC characteristic curves that could be linearized and used in a thermo-economic optimization model based on a Mixed-Integer Linear Programming (MILP) algorithm.

**Keywords:** part-load operation; Carnot battery; energy storage; power-to-power efficiency; organic Rankine cycle; two-stage heat pump; pumped thermal energy storage

check for updates

**Citation:** Nadalon, E.; De Souza, R.; Casisi, M.; Reini, M. Part-Load Energy Performance Assessment of a Pumped Thermal Energy Storage System for an Energy Community. *Energies* **2023**, *16*, 5720. https://doi.org/10.3390/en16155720

Academic Editor: Vedran Mrzljak

Received: 23 June 2023
Revised: 25 July 2023
Accepted: 27 July 2023
Published: 31 July 2023

**Copyright:** © 2023 by the authors. Licensee MDPI, Basel, Switzerland. This article is an open access article distributed under the terms and conditions of the Creative Commons Attribution (CC BY) license (https://creativecommons.org/licenses/by/4.0/).

## 1. Introduction

The current global energy crisis was essentially the result following some key facts such as the post-COVID-19 pandemic economic recovery and the Russia/Ukraine war in February 2022 [1]. This last fact was specifically critical for what concerns the primary energy supply and the consequent energy price sharp growth in Europe. The pitiless energy prices increase [2], in comparison with pre-pandemic levels, and a considerable fossil fuel consumption growth [3] led the European Union (EU) to issue a report [4] with a set of orientations to avoid primary energy shortages in 2023, including the deployment and implementation of renewable energy sources (RES) and technologies. Indeed, this is in agreement with what the scientific community has discussed regarding a scenario where energy systems head toward 100% RES and technologies, including discussions about the role of combined heat and power (CHP) systems in such a scenario [5].

In order to approach a 100% RES scenario, it is imperative to deal with an intrinsic drawback of most renewable energy sources: its intermittent characteristic. This is when energy storage technologies (ESTs) should come into the stage. To have an idea, according to the International Energy Agency (IEA) [6], in a net zero emissions scenario, the current installed grid-scale battery storage capacity would have to increase by a factor of 44 by 2030. Such a fact demonstrates the need to further develop EST. Two of the main research lines in this sense, found in the literature, are phase change materials (PCM) and power-to-power (P2P) technologies. PCM technologies have been investigated for both enhancement of themselves [7,8] and specific applications for the improvement of energy systems' efficiency [9]. P2P ESTs have been largely considered in the literature as an attractive way to deal with RES drawbacks. For instance, according to Katsaprakakis et al. [10], different types of P2P EST could be employed in different scenarios, including the maximization of RES utilization. Several types of P2P EST are considered throughout the literature [10–13], including pumped hydro storage (PHS), compressed-air energy storage (CAES), electrochemical batteries, power-to-gas-to-power (P2G2P), superconducting magnetic energy storage (SMES), and electrochemical double-layer capacitors (EDLCs). However, as claimed by the same authors, these ESTs present some drawbacks (including geographical constraints and requirement of fossil fuel streams) that prevent them from being implemented in specific applications.

Another P2P EST is the so-called thermo-mechanical energy storage (TMES), which is a category of storage systems in which electricity is stored through a thermo-mechanical process. It essentially combines thermal and mechanical energy storage components with other components, including heat exchangers, turbines, and compressors [14]. In agreement with [14,15], TMES has fundamentally four sub-categories, based on their operation principles: thermal energy storage (TES), compressed-air energy storage (CAES), liquid-air energy storage (LAES), and pumped thermal energy storage (PTES). Each sub-category is divided into different systems, which are based on the combination of components within them. TES uses power to increase the temperature of a specific medium (e.g., by means of electrical resistances), and this heat can be further used directly in an industrial process (in this case, the mechanical devices of the power cycle are absent) or converted back into electricity. CAES systems compress and store air at high pressure levels, while LAES systems store liquefied air at low pressure levels, and both take advantage of that potential energy to further obtain electricity. PTES systems consume electricity to feed an HP and store the produced heat in a TES. Then, the TES feeds a power cycle to reobtain the electricity.

PTES systems have progressively gained attention from the scientific community. One of the main reasons for that is the absence of geographical constraints, which makes it more attractive when compared to the other types of EST, mentioned above. For instance, the work developed by Steinmann et al. [16] divided the PTES types into closed Brayton, closed Brayton with recuperation, reverse Brayton combined with Rankine cycle, subcritical Rankine (with organic fluids, as working fluid), and trans-critical Rankine. In particular, ORC systems have had a considerable diffusion in various fields to make different energy systems more efficient by transforming heat into thermal energy.

For example, Casisi et al. [17] studied the inclusion of an ORC for increasing the energy efficiency of a system with internal combustion engines for ship propulsion.

One of the main highlights from their study is that the PTES systems based on Rankine cycles are able to produce better round-trip efficiency levels when compared to the ones based on Brayton cycles. A further work developed by Dumont and Lemort [18] conducted an investigation through which performance maps were built based on the PTES system heat input: waste heat or ambient air temperature. However, there is a lack of part-load performance data in their study, which is, in fact, their suggestion for future works.

For the past five years or so, the "Carnot Battery" (CB) designation has been used in the literature to refer to some technologies such as PTES and LAES [19–22]. Recently, an interesting collaboration between the IEA and specialists from academia and industry (named "Task 36—Carnot Batteries") [23] has been developed with the aim to assist

the development of novel energy storage systems to support the transition toward an energy system scenario based on renewable sources. In a literature review about CBs, Dumont et al. [22] described innovative technologies, analyzed the involved market, and examined existing prototypes. Then, similarly to [15], PTES is subdivided into Brayton and Rankine types. One of their main conclusions is also the absence of studies analyzing the part-load of CBs, which could be extremely helpful in order to assess the performance deterioration in part-load operation.

From the depicted literature review, one can observe the attention that the scientific community has given to CBs, and more specifically to TI-PTES. They have evaluated important aspects, such as different CB component configurations, the influence of key parameters on CBs performance, and economic assessments. However, to the best of the authors' knowledge, there are no studies on the literature dealing with *in-design* and *off-design* CB models for several different working fluids, providing evaluations about the CB part-load operation and explicitly offering results and discussions on the CB characteristic operation curves. For that reason, this work aims to fill this research gap by:

- Developing the *in-* and *off-design* models to study the performance of a CB.
- Evaluating the CB full-load operation;
- Assessing the performance deterioration of the CB when operating at part load;
- Building the CB characteristic performance curves.

The round-trip efficiency has been assessed for two main scenarios: taking heat from a cold reservoir in the ground and taking heat from a heat storage at 80 °C. The study is developed through a methodology section, two sections describing the *in-* and *off-design* models, and a results section where the main findings are presented and discussed.

## 2. Methodology

A set of previous works from our research group on the Energy Communities (ECs) [24–27] has indicated how such users' clusters could take advantage by sharing the thermal and electrical energies they produce by themselves, but still, in some hours of the day (especially during the nighttime), they have to purchase some amount of electricity from the grid. The optimization data obtained suggested that the installation of thermal storage (TStor) could represent a good improvement for the EC devices used, especially during the warm season, and so, it has been decided to investigate how a CB should alter the EC optimization in a future work. So, this work is a preliminary study about a CB to be installed at the EC location. A hypothesis of beneficial return has been made assuming the implementation of a CB into the community, to contain part of the grid dependency producing electric energy from the thermal one. During the sunlit day hours, electric energy surplus coming from photovoltaic panels (PVps) through a distribution substation (DS), the EC interface with the electric grid, could be used to charge a CB using the electricity to operate an HP that takes the heat from a latent or sensible heat storage to fill a high-temperature heat storage (HTHStor), as depicted in Figure 1a and b, respectively.

Two scenarios have been investigated: in case one, the HP, operated through the excess of electricity produced by the Energy Community (EC) of nine users, takes the heat from cold thermal energy storage (CStor) into the ground, considered at a constant temperature of 12 °C (Figure 2a). In case two, the heat is pumped from the sensible heat thermal storage (Tstor) at the central unit of a District Heating Network (DHN). The Tstor is charged at a temperature of 80 °C (Figure 2b) by a DHN and discharged at 77 °C by the HP itself, raising the round-trip efficiency of the whole CB over the unity (in ideal conditions), just diminishing the work done by the HP [28]. In both cases, the HP charges a latent heat HTHStor, with a phase change temperature of 121 °C. The ORC operates by taking energy from the HTHStor and discharging it into the Cstor, for both scenarios, while partially satisfying the community's electrical demand. Both the HTHStor and the Cstor use water to exchange heat between the working fluids and the phase change materials (PCMs).

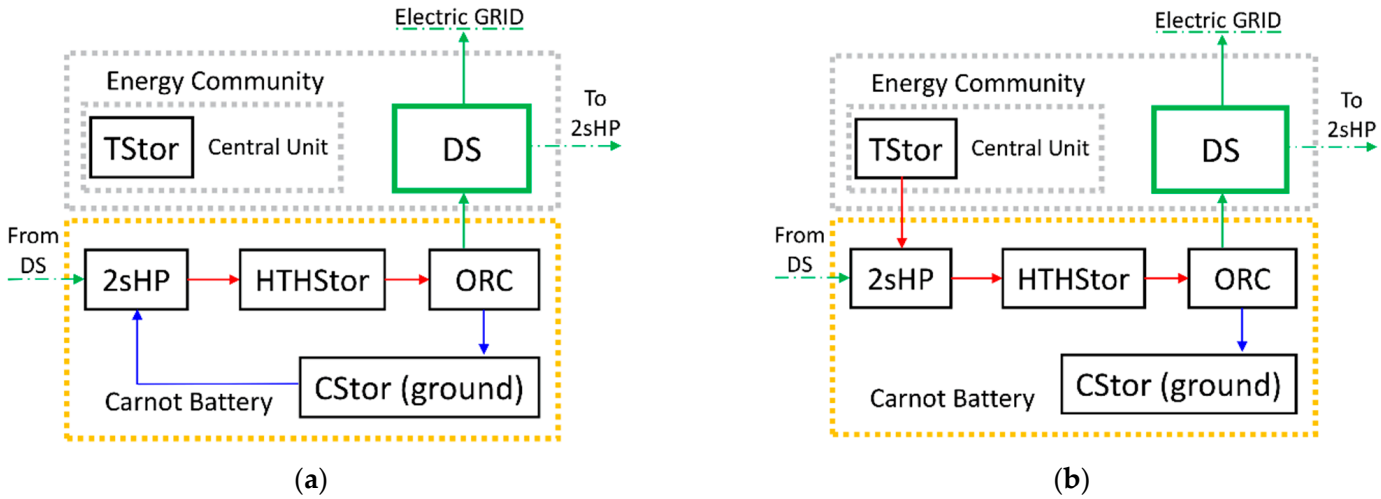


**Figure 1.** The Carnot Battery installed at the Energy Community: (**a**) scenario one, the HP takes the heat from the ground (latent heat thermal storage); (**b**) scenario two, the HP takes the heat from the central unit thermal storage (sensible heat thermal storage).

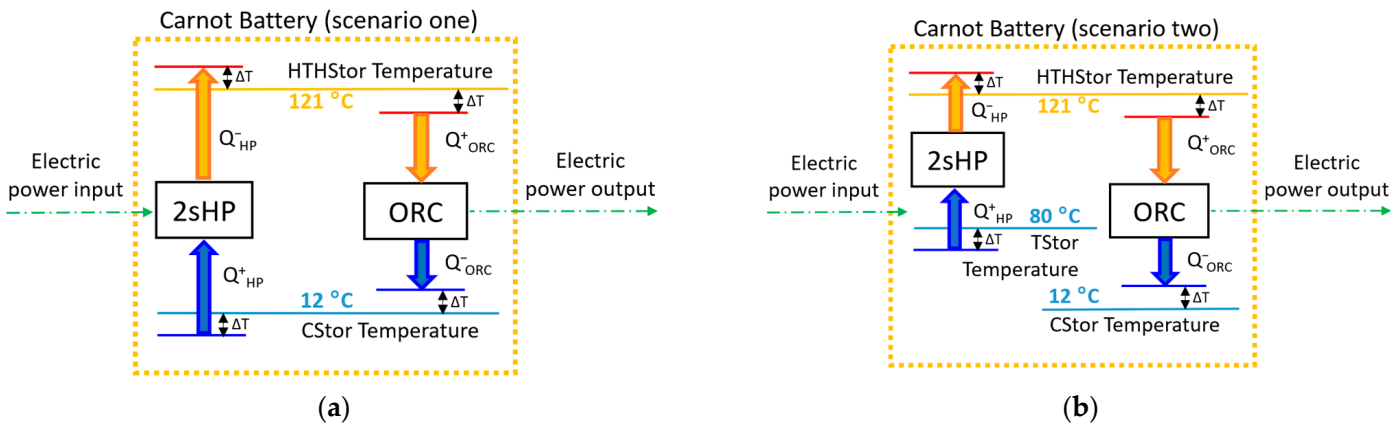


**Figure 2.** The Carnot Battery temperature diagram: (**a**) scenario one, the HP and the ORC work between the same storages; (**b**) scenario two, the devices work between different storages.

Since the energy surplus could not be sufficient to operate the HP at full load for all the charge time periods, a part-load behavior has been implemented in the model about the HP cycle. A similar consideration has been made about the ORC, and the part-load behavior has been considered to take into account the demand satisfaction that occurs when the electric energy from the PVps is not available.

An *in-design* model has been run at working fluid full load to understand the device working limits and perform the calculation about the CB heat exchanger areas. Then, an *off-design* model has been adopted to investigate the part-load dependencies of the physical characteristics of the machines and get the characteristic curves of the HP and the ORC in the CB.

A two-stage HP has been modeled to gain a higher COP with respect to the single-stage HP one. The HP and the ORC cannot work simultaneously, mandatorily, and use two screw compressors (HP) and a screw expander (ORC). In this work, the possibility to operate one of the HP screw compressors in a reversible way as the ORC screw expander has not been considered.

All the heat exchangers (HEXs) for both machines have been sized during the *in-design* project, while an *off-design* analysis has been conducted with the aim to get the HP and ORC characteristic curves about the part-load behavior.

At the beginning of the research presented in this paper, many working fluids have been considered and briefly analyzed in order to find which one would perform better within the defined temperature range for both the case studies.

Once the better fluids have been identified, they have been considered to flow into both the 2sHP and the ORC, and, once the data about the HP COP and the ORC efficiency have been obtained, a further analysis has been performed using the best-performing fluid for each device.

A PTES CB is a device composed of three kinds of devices: a 2sHP, some TS, and an ORC. Considering the 2sHP and starting from point 1 of Figure 3, the working fluid is entering the first regenerator, where it is superheated. Then, it enters the first compressor (point 2) where its pressure raises to the intermediate pressure (point 3) just before entering the phase separator. The vapor exits the phase separator (point 4) to pass through the second regenerator to get superheated again (point 5). The second compressor raises the working fluid pressure to the condensation pressure. The hot vapor then enters the condenser (point 6), where it exchanges heat with the water coming from the HTHStor and charges the storage, becoming saturated vapor (point 7). The further heat released by the working fluids into the condenser makes the fluid condense, becoming saturated liquid (point 8). The fluid enters the second regenerator to exchange heat and reach the sub-cooled condition (point 9). It passes through a lamination valve to adiabatically expand and lower its pressure (point 10). Entering the phase separator again, the fluid liquid fraction is split and leaves the separator to enter into the first regenerator (point 11). Once it has exchanged some heat, the fluid passes through another lamination valve (from point 12 to 13) to reduce its pressure to the evaporation pressure. The fluid enters the evaporator, where it absorbs heat from the water coming from the ground storage (CSTor) in the first scenario or from the DHN storage (TStor) in the second. Once the fluid has exited the evaporator, it reaches point 1 and the cycle starts again. Therefore, the 2sHP uses an electric energy source (PVps) to charge the HTHStor.

The ORC does the opposite: it discharges the HTHStor to produce electric energy and satisfy the EC demand. Starting from point 21, a pump raises the pressure of the liquid working fluid (point 22) through a regenerator, where the fluid gets heated (point 23). The fluid, successively, enters the economizer (point 124), where it starts absorbing heat from the water coming from the HTHStor. The fluid absorbs heat into the evaporator (point 24), becoming saturated vapor (point 25). Then, the vapor drives the expander, which, connected to a generator, produces electric energy. The exhaust vapor at the expander exit (point 26) is hot enough to enter the regenerator and heat the fluid coming out the pump. Once the fluid comes out of the regenerator (point 27), it enters the condenser, where it releases heat to the water coming from the ground storage (CStor), firstly de-superheating to saturated vapor (point 28), and successively condensing into saturated liquid that flows out of the condenser (point 21).

The thermo-fluid-dynamics analysis of the exchange between the water and the PCM of the storages has not been performed, but, simply, the constant temperature at which the phase change must take place has been considered in the model. For further details about the thermo-fluid-dynamics of PCM, refer for instance to [29,30].

The preliminary working fluids investigation has been conducted considering an HP with just one stage, and not two, so the HP cycle has to be considered such that, once the working fluid exits the compressor at point 3 (of Figure 3), it enters the condenser at point 6. Therefore, the phase separator, the second regenerator, and the second compressor do not exist.

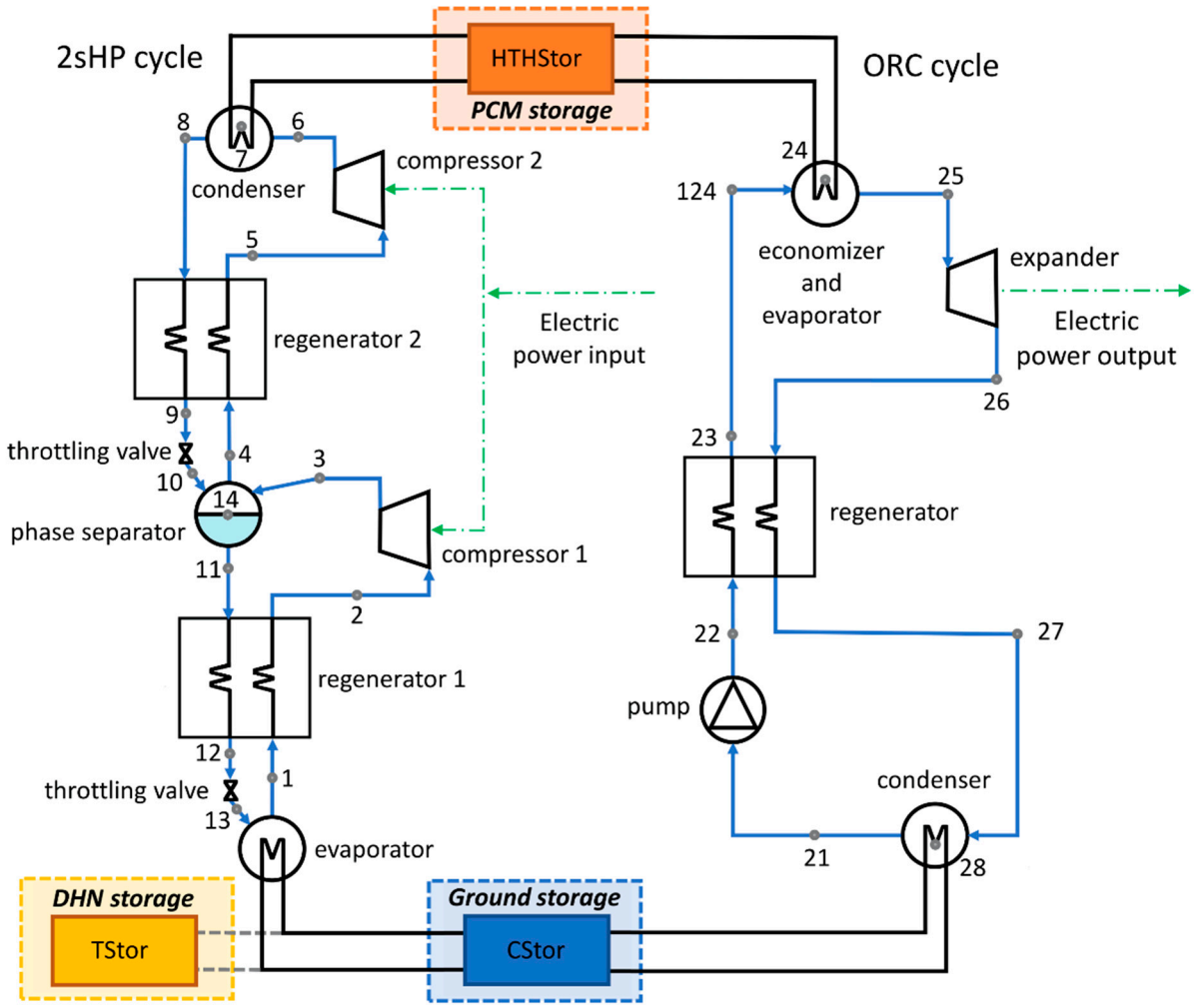


**Figure 3.** The operation diagram of the cycles of the CB for both scenarios. It is worth noting that in the first scenario, both 2sHP and ORC are connected to the ground storage CStor, while in the second scenario, the 2sHP is connected to the storage TStor feed by the EC DHN.

### *2.1. Preliminary Fluids Selection*

Using EES (Engineering Equation Solver (Academic Professional V10.998-3D) by F-Chart Software LLC) [31], several kinds of working fluid have been taken into account (Table 1), in a similar way to the work of Frate et al. [19]. In order to obtain the fluid performance curves about a single-stage HP and an ORC with heat regeneration, a fixed temperature range between the condensation and the evaporation cycle temperatures has been considered (Figures 4 and 5).

**Table 1.** List of the fluids considered with their own critic and saturation temperatures.

| Fluid | Critic Temperature [°C] | Saturation Temperature at P = 1 atm [°C] |
|---|---|---|
| Toluene | 318.6 | 109.9 |
| Isopentane | 187.2 | 27.48 |
| R600 | 152 | −0.87 |
| R600a | 134.7 | −12.01 |
| R1224yd(Z) | 155.5 | 14.27 |
| R1233zd(E) | 165.6 | 17.98 |
| R1234ze(E) | 109.4 | −19.58 |
| R1234ze(Z) | 150.1 | 9.39 |
| R1336mzz(Z) | 171.3 | 33.12 |

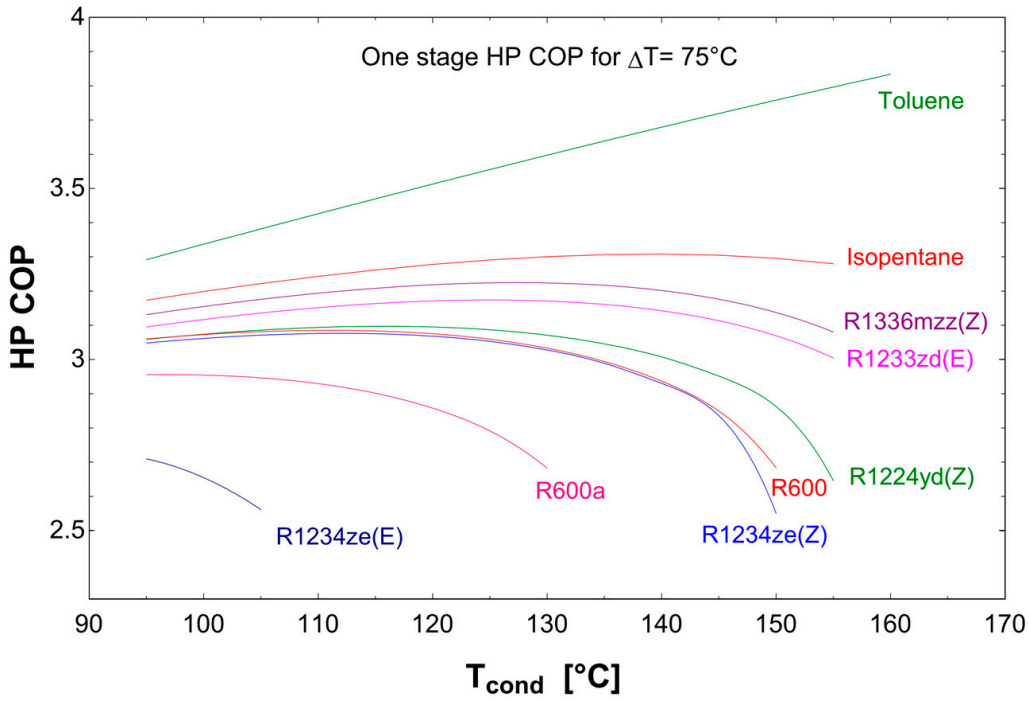


**Figure 4.** The COP performance of the single-stage HP working at a $\Delta T_{HP}$ = 75 °C for several fluids. It is possible to observe that the best performances are those of toluene and isopentane.

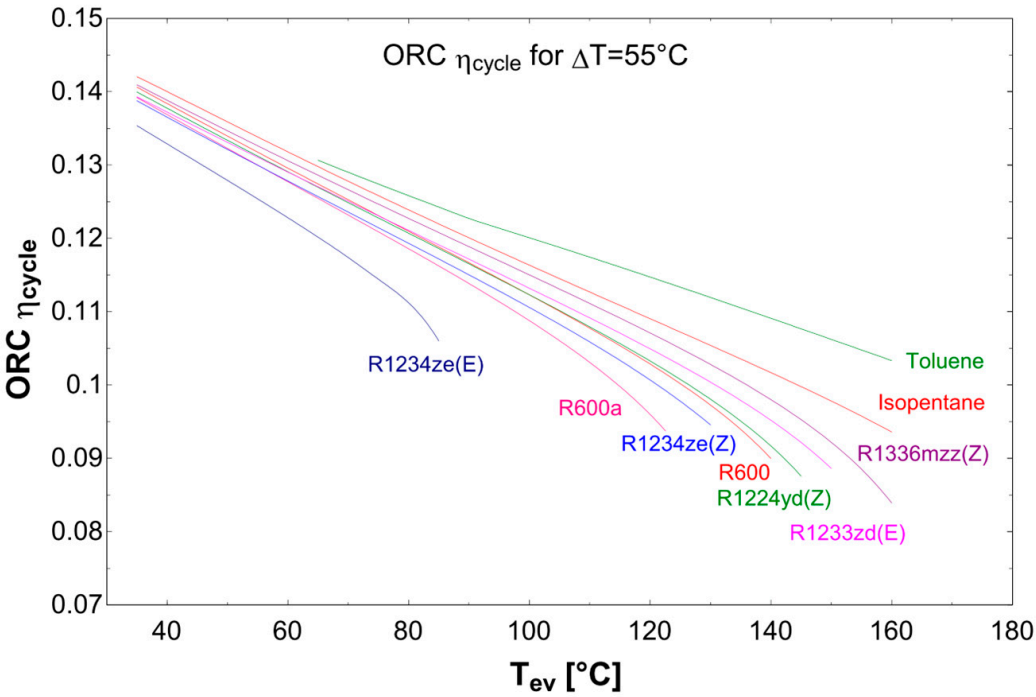


**Figure 5.** The efficiency of the ORC working at a $\Delta T_{ORC}$ = 55 °C for several fluids. It is possible to observe that the best performances are those of toluene and isopentane.

An almost ideal component behavior has been used to perform this investigation, since no pressure drops have been taken into consideration [30], and only a few machine efficiencies not equal to unity have been used, as described in Table 2.

**Table 2.** HP and ORC Efficiencies and efficacies assumed in the preliminary fluids analysis.

| Machine | Compressor/Expander Efficiency | HP/ORC Regenerator Efficacy |
|---|---|---|
| One-Stage HP | 0.7 | 0.8 |
| ORC | 0.88 | 0.8 |
| Two-stage HP [a,1] | 0.7 | 0.8 |
| Two-stage HP [a,2] | 0.7 | 0.3 |

[a] Values for the two-stage HP used in the second part of the preliminary analysis. [1] HP first stage; [2] HP second stage.

Four temperature differences between the highest and the lowest cycle temperatures have been considered for the HP and the ORC to investigate the fluids' performances (Table 3), keeping the lowest temperature at a minimum of 15 °C (near the constant CStor ground temperature of 12 °C) and the highest temperature at a maximum of 160 °C.

**Table 3.** The temperature differences used to investigate the one-stage HP and the ORC performances.

| Machine | $\Delta T_1 = T_H - T_L$ [°C] | $\Delta T_2$ [°C] | $\Delta T_3$ [°C] | $\Delta T_4$ [°C] |
|---|---|---|---|---|
| ORC | 55 | 75 | 95 | 115 |
| One-Stage HP | 75 | 95 | 115 | 135 |

The working fluids' performances have been investigated for several kinds of fluids for the temperature differences reported in Table 3, and the results are reported in Tables 4 and 5 for the fluids that have shown the best performances (HP COP and ORC efficiency).

**Table 4.** The performance of several working fluids for the HP at $T_{cond}$ = 130 °C.

| Fluid | COP at $\Delta T_1$ | COP at $\Delta T_2$ | COP at $\Delta T_3$ | COP at $\Delta T_4$ |
|---|---|---|---|---|
| Toluene | 3.597 | 2.832 | 2.341 | 2.003 |
| Isopentane | 3.300 | 2.612 | 2.175 | 1.876 |
| R1336mzz(Z) | 3.224 | 2.546 | 2.116 | 1.823 |
| R1233zd(E) | 3.171 | 2.517 | 2.100 | 1.814 |
| R1224yd(Z) | 3.071 | 2.444 | 2.045 | 1.772 |

**Table 5.** The performance of several working fluids for the ORC at $T_{ev}$ = 115 °C.

| Fluid | $\eta_{cycle}$ at $\Delta T_1$ | $\eta_{cycle}$ at $\Delta T_2$ | $\eta_{cycle}$ at $\Delta T_3$ | $\eta_{cycle}$ at $\Delta T_4$ |
|---|---|---|---|---|
| Toluene | 0.1161 | 0.1534 | 0.1902 | 0.2252 |
| Isopentane | 0.1107 | 0.1479 | 0.1844 | 0.2206 |
| R1336mzz(Z) | 0.1089 | 0.1456 | 0.1812 | 0.2163 |
| R1233zd(E) | 0.1071 | 0.1434 | 0.1769 | 0.2105 |
| R1224yd(Z) | 0.1057 | 0.1410 | 0.1756 | 0.2098 |

As shown in Figure 4, for the HP, the best performances are those relative to the fluids *isopentane*, and *toluene*, as well as for the ORC, in Figure 5.

### *2.2. Two-Stage HP Optimization*

After an initial evaluation of a single-stage device, a further investigation has been undertaken on a dual-stage HP with two heat regeneration processes. In such a configuration, an optimization on the 2sHP COP has been carried out by varying the intermediate pressure (see Equation (9)), gaining a rise of about 4% of the performance as a mean value.

The latter COP optimization has been performed in EES, disabling Equation (9) (see Section 3.1) in the model and using the optimization function tool that uses a recursive quadratic approximation algorithm of the software itself. In Figures 6 and 7, it is possible to observe how the two-stage HP optimized COP and the ORC efficiency vary by changing the ΔT considered. Toluene is used as an example of working fluid.

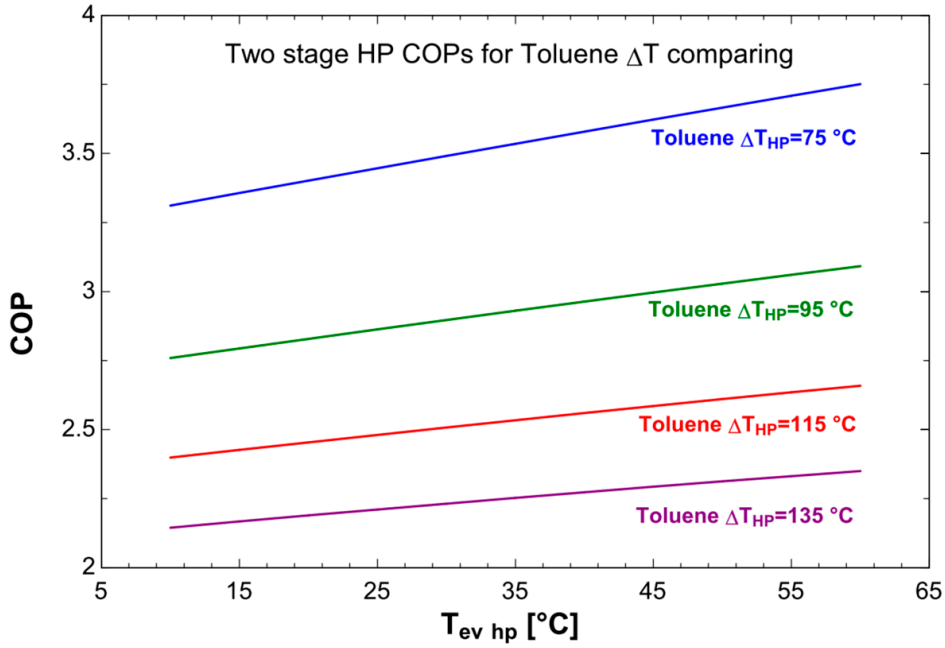


**Figure 6.** Two-stage HP optimized COP for toluene taking into account different cycle temperature differences.

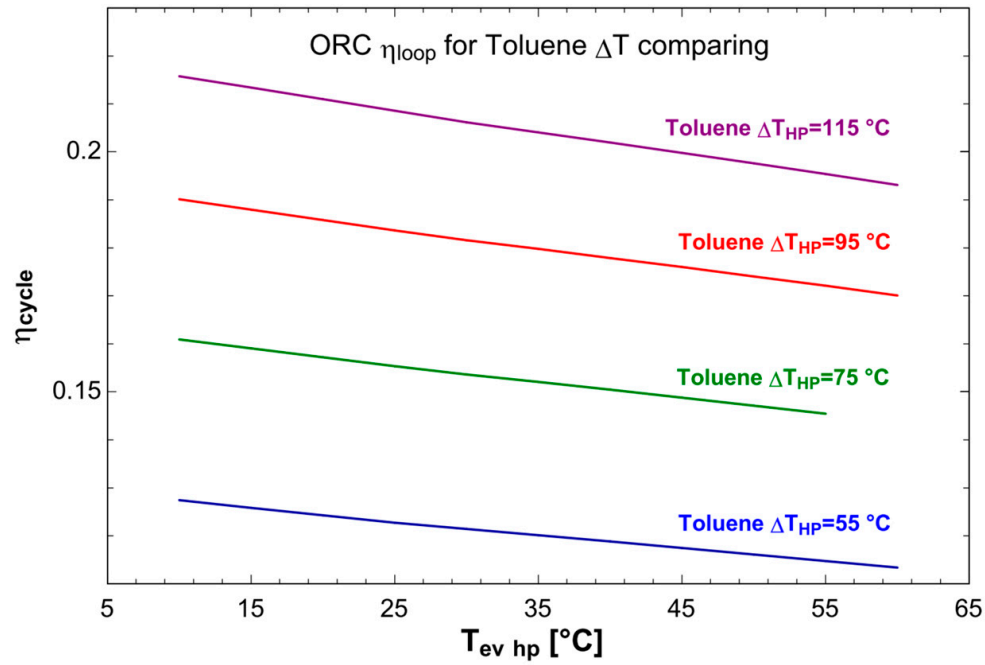


**Figure 7.** ORC efficiency for toluene taking into account different cycle temperature differences.

As expected, the COP of the HP increases when the evaporation temperature $T_{ev}$ increases and when the $\Delta T_{HP}$ decrease (Figure 6), whilst the ORC efficiency ($\eta_{cycle}$) increases when $\Delta T_{ORC}$ increases and $T_{cond}$ decreases (Figure 7). Notice that in both Figures 6 and 7, $T_{ev}$ and $\Delta T_{HP}$ have been used to allow a simultaneous reading of the two figures, $T_{ev}$ and $\Delta T_{HP}$ of the HP being directly linked to $T_{cond}$ and $\Delta T_{ORC}$ of the ORC, respectively, through the values of the pinch-points $\Delta T$ = 5 °C, as shown in Figure 2a.

Finally, the CB round-trip efficiencies $\eta_{Loop}$ have been calculated through Equation (1) for both scenarios (where the storage efficiency $\eta_{Storage}$ is considered equal to one), and the results are shown in Figure 8.

$$\eta_{Loop} = \eta_{ORC} \cdot COP_{HP} \cdot \eta_{Storage} \quad (1)$$

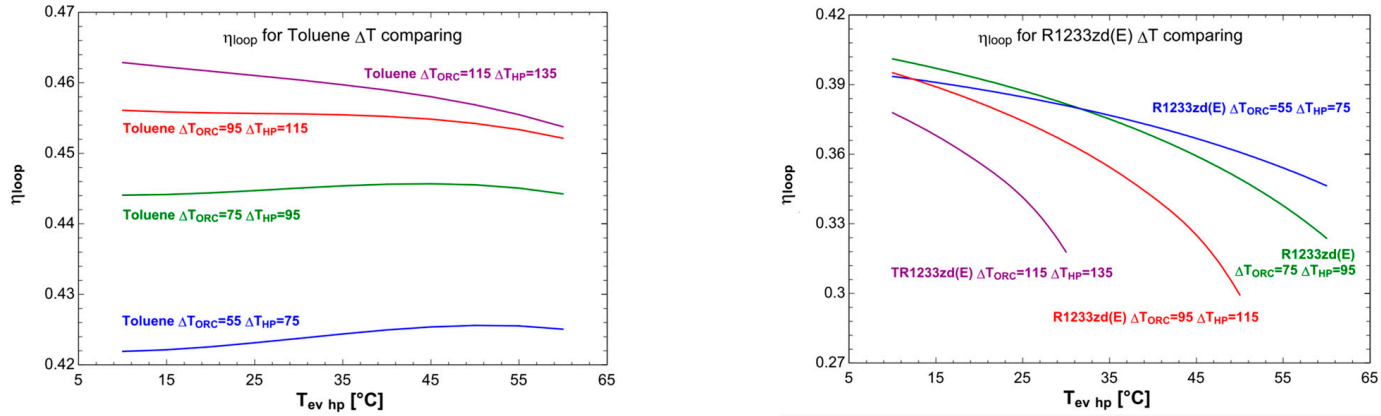


(**a**) (**b**)

**Figure 8.** Round-trip efficiency at the cycle temperature difference considered: (**a**) for toluene; (**b**) for R1233zd(E).

By using toluene as the working fluid (Figure 8a), the resulting round-trip efficiency $\eta_{loop}$ appears to be weakly affected by the evaporation temperature $T_{ev}$ in the considered interval, whilst it increases when $\Delta T_{HP}$ increases, but the increment is sensibly smaller for the higher values of the last parameter. For the working fluid R1233zd(E) (Figure 8b), the maximum values of the $\eta_{loop}$ are obtained at the minimum temperature $T_{ev}$ (about 10 °C or less) and with the temperature increment of the HP in the range $\Delta T_{HP}$ = 75–115 °C. In these conditions, Figure 8b shows $\eta_{loop}$ = 0.39–0.40.

As stated in the introduction, two scenarios have been evaluated. The first one considers that the HP removes heat from a cold ground storage at a constant temperature of 12 °C. In this situation, the round-trip efficiency of the CB in an almost ideal case is about 45%, and it has been calculated thanks to Equation (1) considering the full-load operation.

The second scenario considers that the 2sHP takes the heat from the central unit TStor at about 80 °C. Doing so, the work done by the 2sHP is much less than that in the first situation, and so, the round-trip efficiency, computed as in the almost ideal cases of the previous scenario, rises to 149%.

With the aim of using the same HTHStor temperature of the PCM for both scenarios, a temperature of about 120 °C has been identified, allowing a maximum temperature for the HP cycle of about 130 °C. Despite this initial analysis seeming to indicate the toluene as the best working fluid choice (see Figures 4 and 5), the saturation pressure of the toluene at temperatures near the CStor temperature of the first scenario is about 0.014 bar (Figure 9). The 2sHP evaporator should thus work under high vacuum conditions. Hence, R1336mzz(Z) and R1233zd(E) have been selected as the working fluid for the first scenario for both machines. On the other hand, toluene, at the temperatures considered in the second scenario, could be preferred as a working fluid for the 2sHP, while the ORC could use R1336mzz(Z) and R1233zd(E), since it works even at a condensation temperature of 17 °C. Isopentane has been disregarded because of its low flash point, while toluene is normally used by some companies that produce ORC machines, like the European Triogen [31].

Further discussion about the working fluids selection is reported in Section 5.

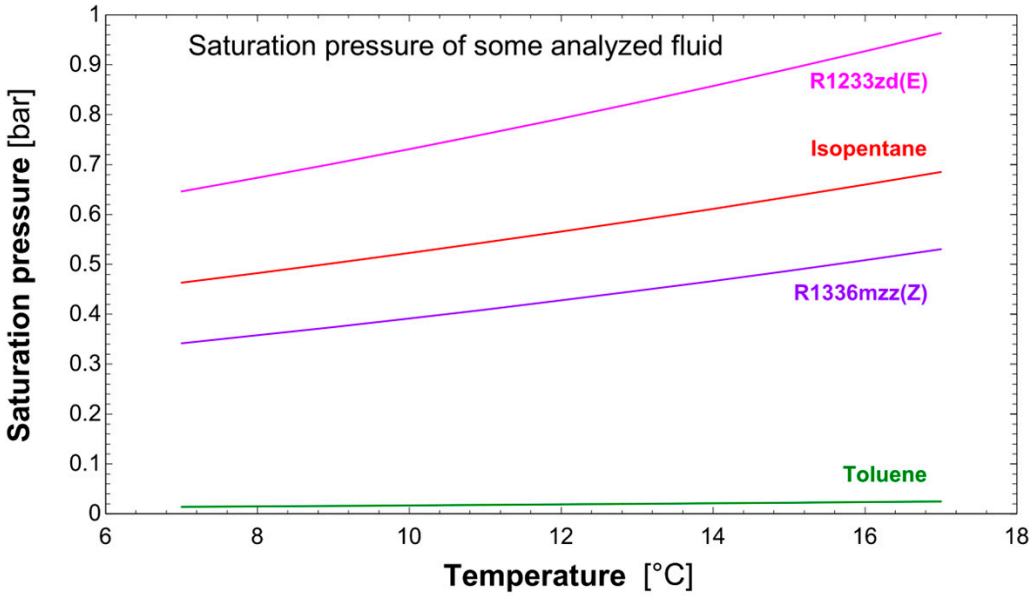


**Figure 9.** The saturation pressures for the best-performing fluids analyzed. Please note how the toluene has a very low saturation pressure value compared with those of the other fluids.

## 3. Design Models

In order to get an *off-design* model of the CB and the characteristic curve of the machines, a preliminary *in-design* steady-state model has been developed to size the heat exchangers surfaces between the machines and the two thermal storages. The *in-design* model is described in the following subsections.

HP compressors and the ORC expander are considered to be screw machines, and no pressure drops have been taken into account for them, nor for heat exchangers and the ORC pump, as done by Eppinger et al. [30].

### *3.1. HP Model*

The HP is a two-stage one, driven by screw compressors. It operates between condensation and evaporation temperatures and with different working fluids depending on the considered scenario. In the first scenario, consistently with the preliminary analysis, the condenser temperature is 130 °C, and the evaporator temperature is 7 °C, with a $\Delta T_{HP}$ = 123 °C, while in the second scenario, the HP condenser temperature remains at 130 °C, and the HP evaporator temperature is set at 75 °C, with a $\Delta T_{HP}$ = 55 °C. The first stage considers a 0.8 regenerator efficacy and a compressor efficiency of 0.7, while the second stage has the same compressor efficiency and a 0.3 regenerator efficacy (see Table 6 for all the assumed HP data) to lower the work of the compressor.

**Table 6.** Compressor efficiencies and regenerators efficacies assumed for the two-stage HP at full load.

| Case | HP Stage | Regenerator Efficacy $\varepsilon_{rig}$ | Isentropic Efficiency $\eta_{is}$ | Electrical Efficiency $\eta_{el}$ | Mechanical Efficiency $\eta_{mec}$ |
|---|---|---|---|---|---|
| 1 and 2 | 1 | 0.8 | 0.82 | 0.97 | 0.94 |
| | 2 | 0.3 | 0.82 | 097 | 0.94 |

The HP cycle diagrams for the two scenarios are shown in Figure 10a,b.

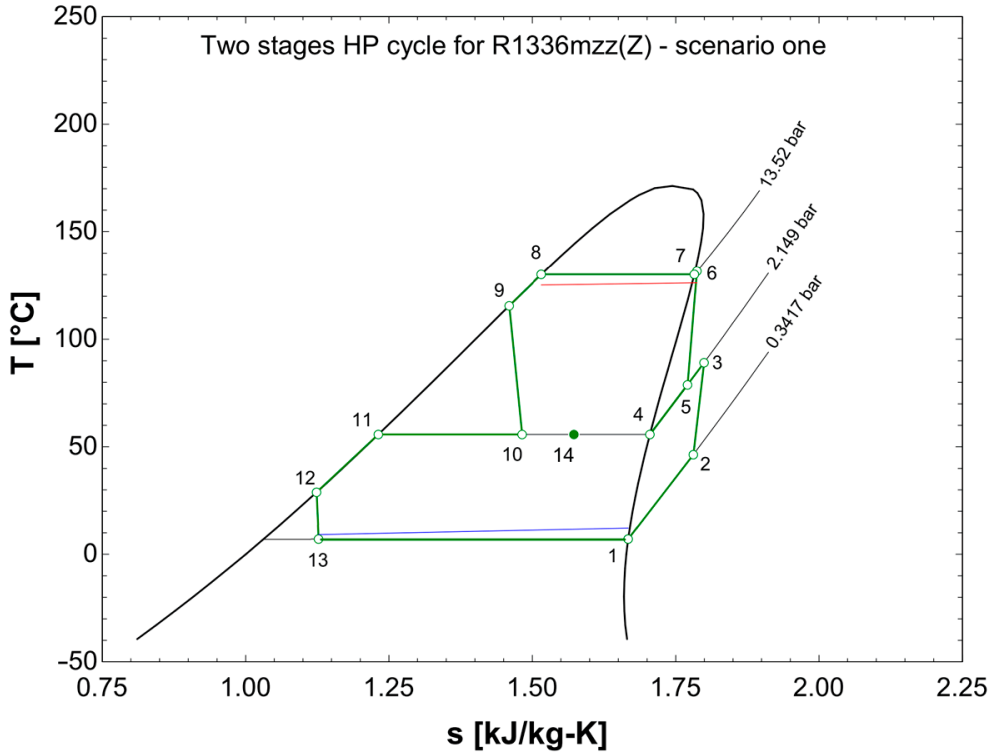


(**a**)

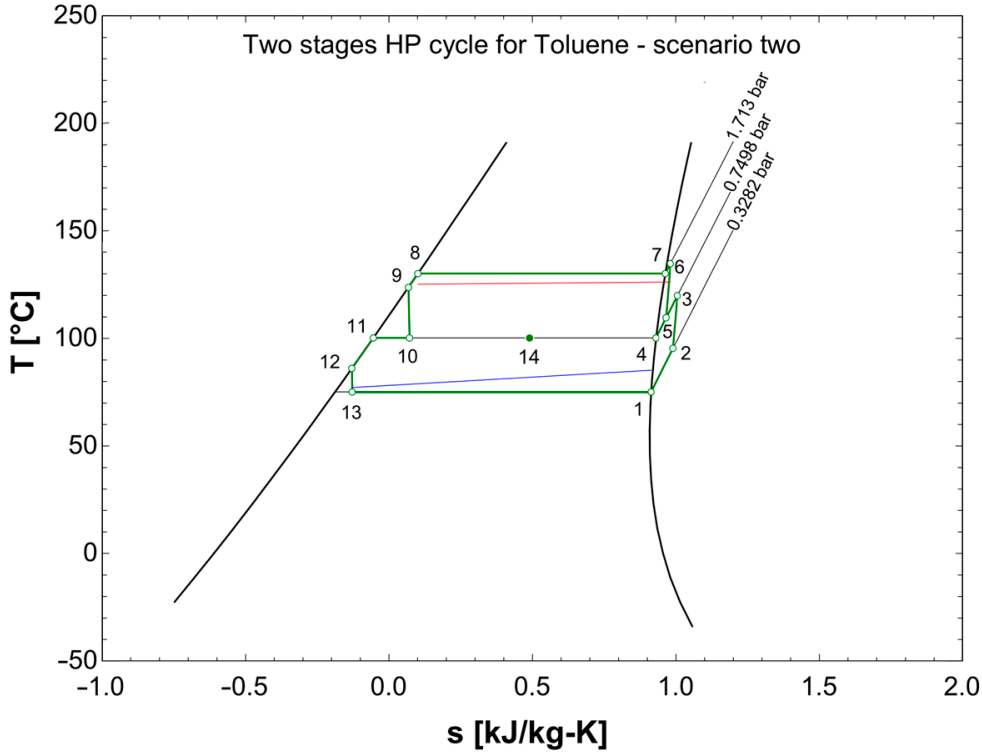


(**b**)

**Figure 10.** (**a**) The HP cycle in scenario one with R1336mzz(Z) as the working fluid; (**b**) The HP cycle in scenario two with toluene as working fluid. Point 14 represents the separation of the two fluid phases at the intermediate exchangers. The working temperature profiles for the thermal storages are shown in red and blue, for high and low temperatures, respectively.

Referring to Figure 10a,b, the regenerator 1 efficacy is described by the following Equation (2):

$$\varepsilon_{rig1} = \frac{(h_2 - h_1)}{(h_{2*} - h_1)} \tag{2}$$

where $\varepsilon_{rig1}$ is the regenerator efficacy, $h_i$ is the specific enthalpy of the $i$-th cycle point, and $h_{2*}$ is the enthalpy calculated at the saturation temperature of the intermediate pressure (see Equation (8)) and at the evaporation pressure. The efficacy of regenerator 2 of the second stage has been evaluated by changing the subscripts of the cycle points accordingly with Figure 10, considering the cycle point numbers 4 and 5 and the specific enthalpy $h_{5*}$ calculated at the condensation temperature and at the intermediate pressure (see Equation (8)).

Both the regenerators superheat the saturated vapor so that it is free of droplets before entering the compressors, allowing them to run safely.

The isentropic efficiency of the HP first-stage compressor has been defined as:

$$\eta_{is_comp1} = \frac{(h_{3is} - h_2)}{(h_3 - h_2)} \tag{3}$$

where $h_{3is}$ is the specific enthalpy of point 3 for an isentropic compression, and the one about the second-stage compressor has been defined by changing the subscript of Equation (3) accordingly with the HP cycle of Figure 10.

Regarding the work absorbed by the two HP compressors, their efficiencies have been modeled through Equation (4):

$$W_{comp1} = \frac{\dot{m}_{ev} \cdot (h_3 - h_2)}{(\eta_{comp1})} \tag{4}$$

where $W_{comp1}$ is the work by the compressor of the first stage, $\dot{m}_{ev}$ is the mass flow of the working fluid flowing through the HP evaporator, $h_i$ represents the specific enthalpy of the $i$-th point of the cycle, and $\eta_{comp1}$ is the compression efficiency expressed by Equation (5):

$$\eta_{comp1} = \eta_{el1} \cdot \eta_{mec1} \tag{5}$$

The compression work $W_{comp2}$ of the second stage has been modeled through Equation (6):

$$W_{comp2} = \frac{\dot{m}_{cond} \cdot (h_6 - h_5)}{(\eta_{comp2})} \tag{6}$$

where $\dot{m}_{cond}$ is the mass flow through the HP condenser.

The value of HP compressors' total work $W_{comp_tot}$ (Equation (7)) and ORC maximum output have been imposed according to Table 7 for the two considered scenarios.

$$W_{comp\ tot} = W_{comp1} + W_{comp2} \tag{7}$$

**Table 7.** HP total input power and ORC net output power for the two case study scenarios.

| Scenario | HP Total Input Power [kW] | ORC Net Output Power [kW] |
|---|---|---|
| 1 | 200 | 70 |
| 2 | 85 | 70 |

Those values are related to the EC needs presented in De Souza et al. [24]. The same values can be scaled up two–three times by enlarging the sizes of the components, or up to ten–twenty times by using a cluster of components in parallel.

Since the *in-design* model has been developed in order to successively run an *off-design* one, working at part-load, the mechanical compressors' efficiencies have been described so they can change with the variation of the part-load by means of the part-load factor $\alpha$: this situation is described in the following Section 4.1.

About the two flows of the HP working fluid, $\dot{m}_{ev}$ and $\dot{m}_{cond}$, they have been computed by the enthalpy balance at the HP intermediate exchanger (represented by point 14 in Figure 10), once the HP input power has been set up, thanks to Equation (8):

$$\dot{m}_{ev} \cdot h_3 + \dot{m}_{cond} \cdot h_{10} = \dot{m}_{ev} \cdot h_{11} + \dot{m}_{cond} \cdot h_4 \quad (8)$$

The condensation and evaporation pressure are the saturation pressures at the condensation and evaporation temperatures, respectively. In the first scenario, the latter are $T_{cond_hp}$ = 130 °C and $T_{ev_hp}$ = 7 °C, while in the second one, they result to be $T_{cond_hp}$ = 130 °C and $T_{ev_hp}$ = 75 °C. The intermediate pressure has been evaluated by Equation (9):

$$p_{int} = \sqrt{(p_{eva_hp} \cdot p_{cond_hp})} = p_3 = \sqrt{(p_1 \cdot p_7)} \quad (9)$$

Because of the two-stage HP, it has been chosen to use a separated ORC instead of considering a reversible machine, which is the case of a single-stage HP and an ORC using the same screw compressor/expander as a reversible component, as carried out by Eppinger et al. [30].

### 3.2. ORC Model

The ORC model developed has a screw expander and operates between a condenser temperature of 17 °C and an evaporator temperature of 113 °C, with a $\Delta T_{ORC}$ = 96 °C, considering R1336mzz(Z) and R1233zd(E) as the working fluid for both the studied scenarios.

The machine works between the condenser pressure, that is the saturation pressure at condenser temperature, and the evaporator pressure, i.e., the saturation pressure at evaporator temperature.

The cycle is depicted in Figure 11, and every cycle point is named after a number.

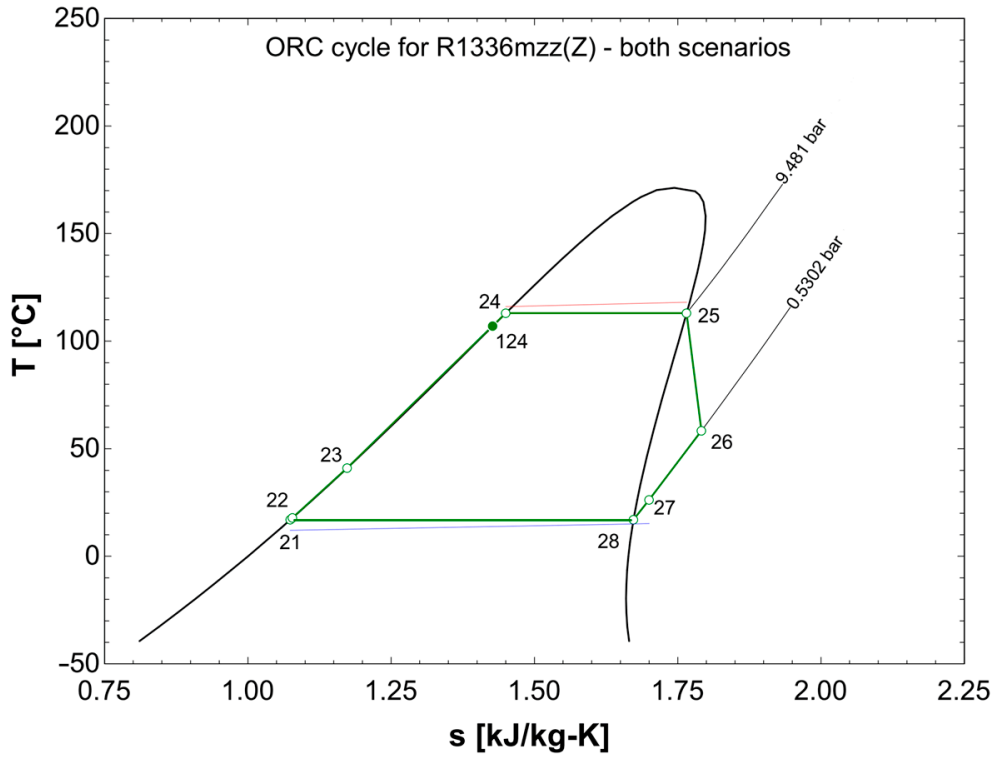


**Figure 11.** The ORC cycle for both scenarios with R1336mzz(Z) as the working fluid. Point 124 represents the economizer outlet. The working temperature profiles for the thermal storages are shown in red and blue, for high and low temperatures, respectively.

The ORC presents a regenerator that exchanges heat between the expander outlet and the pump outlet with an efficacy of 0.8. At full load (see Section 3.1 for the part-load ORC behavior), the screw expander isentropic efficiency is about 0.79, coming from Equation (10) and the values reported in Table 8:

$$\eta_{exp} = \eta_{el_exp} \cdot \eta_{mec_exp} \tag{10}$$

**Table 8.** Expander and pump efficiencies and regenerator efficacy assumed for the ORC at full load.

| Device | Regenerator Efficacy $\varepsilon_{rig}$ | Isentropic Efficiency $\eta_{is}$ | Electrical Efficiency $\eta_{el}$ | Mechanical Efficiency $\eta_{mec}$ |
|---|---|---|---|---|
| Expander | - | 0.82 | 0.97 | 0.94 |
| Pump | - | 0.85 | 0.97 | 0.70 |
| Regenerator | 0.80 | - | - | - |

The isentropic expander efficiency has been defined through Equation (11):

$$\eta_{is_exp} = \frac{(h_{25} - h_{26})}{(h_{25} - h_{26is})} \tag{11}$$

where $h_i$ is the specific enthalpy of the $i$-th cycle point (as depicted in Figure 11).

On the other hand, the isentropic pump efficiency is given by Equation (12):

$$\eta_{is_pump} = \frac{(h_{22is} - h_{21})}{(h_{22} - h_{21})} \tag{12}$$

Lastly, the ORC regenerator efficacy is as in Equation (13):

$$\varepsilon_{rig} = \frac{(h_{26} - h_{27})}{(h_{26} - h_{27*})} \tag{13}$$

where the specific enthalpy $h_{27*}$ has been evaluated at the condensation pressure and at the temperature of the pump outlet (point 22 of Figure 11).

The works related to the expander and the pump are illustrated in Equations (14)–(16), as follows:

$$W_{gross_exp} = \dot{m}_{orc} \cdot (h_{25} - h_{26}) \cdot \eta_{exp} \tag{14}$$

$$W_{pump} = \frac{\dot{m}_{orc} \cdot (h_{22} - h_{21})}{(\eta_{pump})} \tag{15}$$

$$W_{net_exp} = W_{gross_exp} - W_{pump} \tag{16}$$

where $W_{gross_exp}$ and $W_{net_exp}$ are the gross and net work done by the ORC, respectively, and $\dot{m}_{orc}$ is the working fluid mass flow into the ORC.

Finally, the ORC presents an economizer, which is responsible for the pre-heating of the fluid entering into the evaporator. At the outlet of the economizer has been set up an approach-point, described in the following Section 3.6.4.

### *3.3. High-Temperature Thermal Storage Hypothesis*

A latent heat HTHStor (Figure 1) keeps its temperature at about 121 °C using a salt mixture of nitrates, $LiNO_3/NaNO_3/KNO_3$, as a PCM and water as a medium to exchange heat with the HP condenser and the ORC evaporator. The latent heat material has been selected considering the PCM temperature, as stated in Table 9, after a search in the literature.

The water from the HTHstor has been considered flowing into the HP condenser and into the ORC evaporator at a pressure of 5 bar, in order to keep the water in liquid phase for the adopted temperatures.

Finally, the storage dimensions have been left free in size so that they can adapt to the user's demand.

**Table 9.** Phase change materials and their latent heat temperatures from several authors.

| Compound | Melting Temperature [°C] | Heat of Fusion [kJ/kg] | Source |
|---|---|---|---|
| $KCl/LiNO_3$ | 165.6 | 201.7 | S. A. Mohamed [32] |
| A164 * | 164 | 306 | H. Ge et al. [33] |
| $NaNO_3/KNO_3/NaNO_2$ | 142 | - | S. A. Mohamed [32] |
| $Bi_{58}Sn_{42}$ | 138 | 44.8 | H. Ge et al. [33] |
| $LiNO_3/NaNO_3/KNO_3$ | 121 | - | S. A. Mohamed [32] |
| $MgCl_2{\cdot}6H_2O$ | 117 | 168.6 | M. M. Farid et al. [34] |
| $Bi_{52}Pb_{30}Sn_{18}$ | 96 | 44.8 | S. A. Mohamed [32] |
| $(NH_4)Al(SO_4)_2{\cdot}12H_2O$ | 95 | 269 | S. A. Mohamed [32] |
| E89 * | 89 | 163 | H. Ge et al. [33] |
| E83 * | 83 | 152 | H. Ge et al. [33] |

Compounds marked with (*) are products from EPS Ltd, UK. (see H. Ge et al. [33]).

### *3.4. District Heating Network Thermal Storage Hypothesis*

The EC has been provided with a central unit in which there is a sensible heat thermal storage (TStor) fed through the DHN of the community, by cogenerators (micro gas turbine (MGT) and internal combustion engine (ICE)) and the solar thermal panels (STPs) of the central unit itself.

The studied second scenario considers the TStor as "cold" storage for the HP, from which the HP evaporator takes the heat at 80 °C to pump it into the HTHStor by means of the HP condenser. The water flowing in the HP evaporator leaves the HEX at 77 °C.

### *3.5. Cold Thermal Storage Hypothesis*

Cold thermal storage is a latent heat storage that uses the ground as a heat reservoir at 12 °C constant temperature.

When the HP is pumping the heat from the cold thermal storage (CStor) to the HTHStor, the first case scenario is represented. The ORC exchanges heat between the CStor and the HTHStor in both case scenarios.

### *3.6. Heat Exchangers Sizing*

In Section 4, we will describe the *off-design* working of the CB model, used to obtain the characteristic curves of the HP and ORC when they run in part-load situation. To do so is fundamental to calculate the area of each HEX present in the whole machine.

Every HEX of the CB has been imagined as a shell and tube device, in counter-flow and with one pass, with the tubes displaced in triangular pitch. The mathematical equations used vary based on the kind of HEX considered. There is no distinction in the mathematical description of HP and ORC HEXs. The fluids used in the two scenarios are the selected working fluid and water.

In order to calculate the HEX areas, the overall conductance $UA_j$ of the $j$-th HEX has been divided by the overall heat exchange coefficient $U_j$, which in turn has been approximated with Equation (17), which does not take into account the thickness of the tubes:

$$U_j = \left(\frac{1}{h_t} + \frac{1}{h_s}\right)_j^{-1} \tag{17}$$

where $h_t$ and $h_s$ are the convective heat transfer coefficients of the fluid on the tube side and on the shell side, respectively. The latter coefficients have been computed using the Nusselt number definition and other correlations described in the following subsections. The values of the overall conductance, $UA_j$, have been obtained through the logarithmic mean temperature difference (LMTD) as described in Section 3.6.2.

#### 3.6.1. Regenerator Models

Every regenerator has been described using the equations found in Nitsche and Gbadamosi [35].

The working fluid flowing through the regenerative HEXs is the same for both the shell and the tubes. The hotter fluid is considered passing through the shell, the colder through the tubes.

In order to obtain the convective heat transfer coefficients, the expression of Nusselt numbers for turbulent flows in Equations (18) and (19) have been adopted:

$$Nu_t = 0.023 \cdot Re^{0.8} Pr^{\left(\frac{1}{3}\right)} \tag{18}$$

$$Nu_s = 0.196 \cdot Re^{0.6} Pr^{\left(\frac{1}{3}\right)} \tag{19}$$

where $Re$ is the Reynolds number and $Pr$ the Prandtl number, while the subscripts $t$ and $s$ stand for tubes and shell sides, respectively, under the hypothesis of turbulent flows.

### 3.6.2. Evaporators Models

The heats exchanged in the HP and ORC evaporators, namely $Q_{ev_hp}$ and $Q_{ev_orc}$, have been assessed through the Equations (20) and (21), accordingly with Figures 10 and 11:

$$Q_{ev_hp} = \dot{m}_{ev_hp} \cdot (h_1 - h_{13}) \tag{20}$$

$$Q_{ev_orc} = \dot{m}_{orc} \cdot (h_{25} - h_{24}) \tag{21}$$

In order to calculate the values of $UA_{ev_hp}$ and $UA_{ev_orc}$ with the help of Equation (22), the LMTD has been defined accordingly with Equation (23) and Figures 10–12:

$$Q_{ev_j} = UA_{ev_j} \cdot \Delta T_{lm_ev_j} \tag{22}$$

where the $j$-th element is the HP or the ORC, respectively.

$$\Delta T_{lm_ev_hp} = \frac{(T_{43} - T_1) - (T_{44} - T_{13})}{ln\left(\frac{T_{43} - T_1}{T_{44} - T_{13}}\right)} \tag{23}$$

where the LMTD about the ORC evaporator can be obtained properly by changing the Equation (23) subscripts.

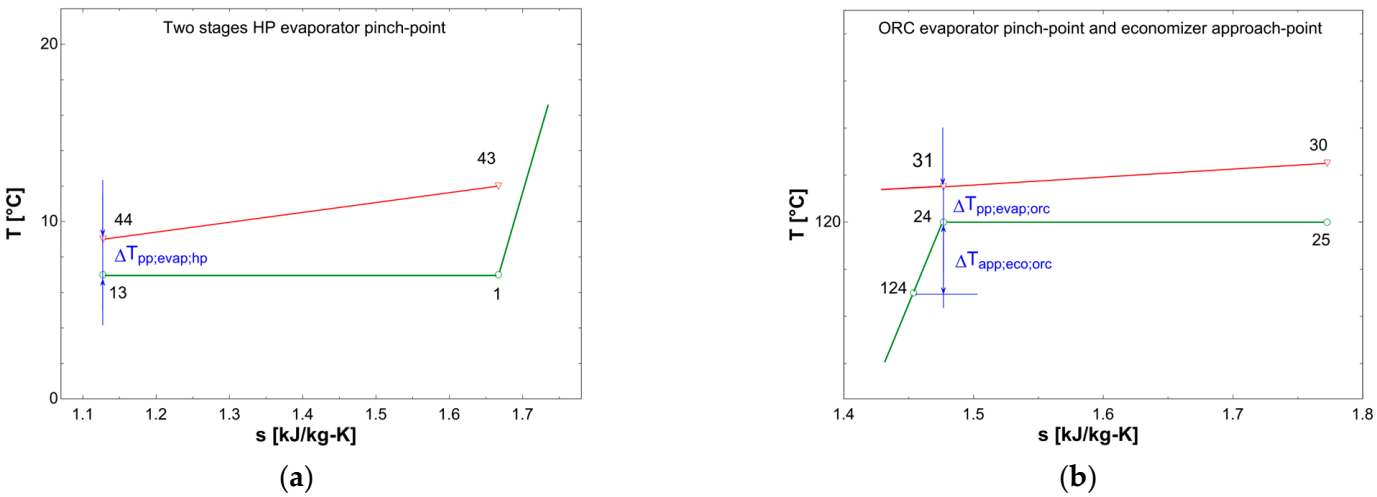


(**a**) (**b**)

**Figure 12.** The evaporator pinch-point representation: (**a**) for the HP; (**b**) for the ORC. The ORC economizer approach-point is depicted as well.

For the HP and ORC evaporators, as well as for their condensers, pinch-point temperature differences have been defined, thanks to Equations (24) and (25) (Figure 12a,b):

$$\Delta T_{pp_ev_hp} = T_{44} - T_{13} \tag{24}$$

$$\Delta T_{pp_ev_orc} = T_{31} - T_{24} \tag{25}$$

where the subscript *pp_ev_j* stands for *pinch-point evaporator* of the *j*-th machine.

The pinch-points about all the HEXs have been defined in the in-design model (see Table 9) in order to allow the *off-design* model to run with the HEX areas fixed and with reduced values of the working fluid flow rates.

The evaporator Nusselt numbers on the tube side have been calculated by means of Equation (18) about the water flowing into the tubes, while the convective heat transfer coefficients on the shell side have been computed using Equations (26) and (27), as described in Serth and Lestina [36] about the working fluid:

$$h_{s_ev} = \alpha_{nb} \cdot F_b \tag{26}$$

$$\alpha_{nb} = \left[55 \cdot \Delta T_{ml}^{\left(\frac{2}{3}\right)} \cdot P_R^{0.12} \cdot \left(-log_{10} P_R\right)^{-0.55} \cdot MM^{-0.5}\right]^3 \tag{27}$$

Here, $\Delta T_{ml}$ is the LMTD of the evaporator, depicted in Figure 12a,b for the HP and the ORC, respectively; *MM* is the molar mass of the fluid flowing in the shell side of the HEX; and $P_R$ is the reduced pressure of the working fluid defined by Equation (28):

$$P_R = \frac{P_{sat_eva}}{P_{CR}} \tag{28}$$

where $P_{sat_eva}$ and $P_{CR}$ are the saturation and the critical pressure of the working fluid into the evaporator.

The factor Fb is instead defined by the following Equation (29):

$$F_b = 1 + 0.1 \cdot \left[\frac{0.785 \cdot D_b}{\left(C_1 \cdot \left(\frac{P_t}{d_o}\right)^2 \cdot d_o\right)} - 1\right]^{0.75} \tag{29}$$

where $d_o$ is the outer tube's diameter, $C_1$ is a geometrical factor based on the triangular pitch $P_t$ of the tube bundle, and $D_b$ is the tube bundle diameter described by Equation (30):

$$D_b = d_o \cdot \left(\frac{N_t}{K}\right)^{\left(\frac{1}{n}\right)} \tag{30}$$

Factors *K* and *n* are tabulated based on the pitch kind and the number of passes $N_p$ of the HEX. All these factors are as follows [36]:

- $P_t$ = 1.25 $d_o$ (chosen by authors);
- $N_p$ = 1 (chosen by authors);
- $C_1$ = 0.866;
- *K* = 0.319;
- *n* = 2.142.

### 3.6.3. Condenser Models

The HP and ORC condensers exchange the heats $Q_{cond_hp}$ and $Q_{cond_orc}$, described by Equations (31) and (32), accordingly with Figures 10 and 11,

$$Q_{cond_hp} = \dot{m}_{cond_hp} \cdot (h_6 - h_8) \tag{31}$$

$$Q_{cond_orc} = \dot{m}_{orc} \cdot (h_{27} - h_{21}) \tag{32}$$

and the LMTD is still described by Equation (23) with the proper subscripts.

The condenser pinch-point temperature differences, instead, have been expressed by Equations (33) and (34) (see Figure 13):

$$\Delta T_{pp_cond_hp} = T_7 - T_{41} \tag{33}$$

$$\Delta T_{pp_cond_orc} = T_{28} - T_{34} \tag{34}$$

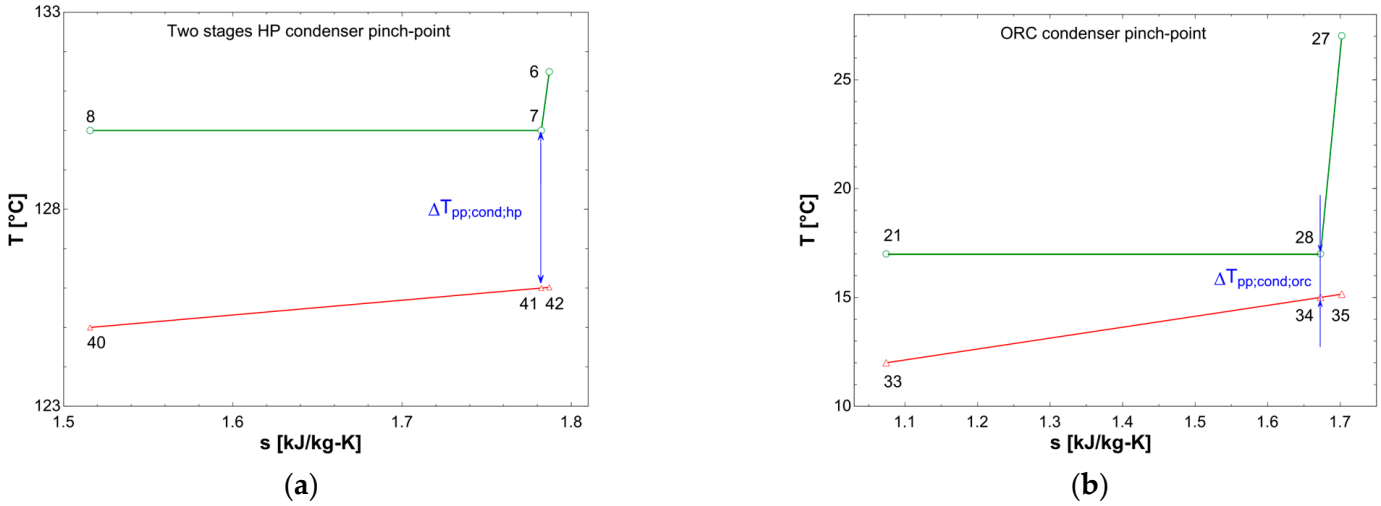


(**a**) (**b**)

**Figure 13.** The condenser pinch-point representation: (**a**) for the HP; (**b**) for the ORC.

Also, for HP and ORC condensers, on the tube side, Equation (17) has been used considering water flowing into the tubes.

The shell side has been modeled through the equations found in the book by Serth and Lestina [36] for condensers with horizontal tubes, taking into account the de-superheating of superheated working fluid vapor [37].

$$h_s = 0.728 \cdot \left( \frac{(k_l^3 \cdot \rho_l \cdot (\rho_l - \rho_v) \cdot g \cdot \lambda')}{(\mu_l \cdot (T_{sat} - T_w) \cdot d_o)} \right)^{\left(\frac{1}{4}\right)} \tag{35}$$

Equation (35) describes how the shell side convective heat transfer coefficient has been calculated. Here, the equation terms are as follows:

- $k_l$ is the liquid working fluid heat conductivity;
- $\rho_l$ is the liquid working fluid density;
- $\rho_v$ is the vapor working fluid density;
- $g$ is the gravity acceleration;
- $\mu_l$ is the liquid working fluid dynamic viscosity;
- $d_o$ is the tube's outer diameter;
- $T_{sat}$ is the saturation temperature of the working fluid;
- $T_w$ should be the tube outer wall temperature, but since we have disregarded the wall thickness, we have used the temperature of the water flowing inside the tubes evaluated as a mean between the inlet and outlet condenser water temperatures;
- $\lambda'$ is the heat defined as follows, by Equation (36) from Serth and Lestina [36]:

$$\lambda' = \lambda + C_{P,\,V} \cdot (T_V - T_{sat}) \tag{36}$$

where $\lambda$ is the latent heat of condensation, and the subscript $V$ stands for *vapor*.

Serth and Lestina [36] specify that "For shell-side condensation of a pure-component vapor in a horizontal E-shell unit, it can be assumed that all the heat is transferred at the saturation temperature in the shell."

Condensate subcooling has been disregarded in the model because it has been considered negligible.

### 3.6.4. ORC Economizer Model

The ORC economizer exchanges the heat $Q_{eco_orc}$, through the Equation (37), accordingly with Figure 11:

$$Q_{eco_orc} = \dot{m}_{orc} \cdot (h_{124} - h_{23}) \tag{37}$$

where the point 124 has been introduced in order to define the economizer approach-point, as follows in Equation (38) (see Figure 12b),

$$\Delta T_{app_eco_orc} = T_{24} - T_{124} \tag{38}$$

and the LMTD is still described by Equation (23) with the proper subscripts.

The ORC economizer has been modeled with the same Nusselt numbers, for both the tube side and shell side, as the regenerators, but considering that into the tubes there is water flowing with thermodynamic properties evaluated at a mean temperature between the inlet and outlet economizer temperatures.

#### 3.6.5. Heat Exchanger Calculated Areas

The HP and ORC heat exchangers areas have been finally computed and are reported in the following Table 10 for the HP and Table 11 for the ORC about the two scenarios:

**Table 10.** HP heat exchanger areas for the two considered scenarios using R1336zz(Z) (scenario 1) and toluene (scenario two).

| HP HEX | Scenario | Area [m$^2$] |
|---|---|---|
| Condenser | 1 | 340.0 |
| | 2 | 175.8 |
| Regenerator 1 | 1 | 85.7 |
| | 2 | 66.8 |
| Regenerator 2 | 1 | 2.2 |
| | 2 | 1.6 |
| Evaporator | 1 | 593.4 |
| | 2 | 201.1 |

**Table 11.** ORC heat exchangers areas for the two scenarios considered using R1336zz(Z).

| ORC HEX | Area [m$^2$] |
|---|---|
| Condenser | 457.1 |
| Regenerator | 148.8 |
| Economizer | 7.4 |
| Evaporator | 50.2 |

## 4. Off-Design Models

### *4.1. Part-Load Mass Flows and Machine Efficiencies*

As stated in the introduction, a part-load working behavior has been considered for both the HP and the ORC, through the adoption of a part-load factor $\alpha$, which can vary from the full-load conditions ($\alpha$ = 1) to the inactive machine ($\alpha$ = 0). The part-load operation affects the HP compressors and the ORC expander efficiency in the ways described by Eppinger et al. [30] and Liu et al. [38].

The variation of working fluid mass flows is reduced from full load to part-load using Equations (39) and (40):

$$\dot{m}_{orc_pl} = \alpha \cdot \dot{m}_{orc_fl} \tag{39}$$

$$\dot{m}_{ev_hp_pl} = \alpha \cdot \dot{m}_{ev_hp_fl} \tag{40}$$

where the subscripts *fl* and *pl* mean *full load* and *part-load*, respectively.

The part-load factor $\alpha$ has been varied between 1 and about 0.25.

The mass flow in the HP second stage $\dot{m}_{ev_hp_pl}$ is calculated by means of enthalpy balance Equation (8) at the HP intermediate exchanger.

Equations (41) and (42), which regard the overall compressor and expander efficiencies, consider the mechanical efficiencies varying with the part-load factor $\alpha$, as described by Equation (11) in Liu et al. [38], becoming the following equations:

$$\eta_{el_comp_pl} = \eta_{el_comp_fl} \cdot \eta_{mec_pl}(\alpha) \tag{41}$$

$$\eta_{el_exp_pl} = \eta_{el_exp_fl} \cdot \eta_{mec_exp_pl}(\alpha) \tag{42}$$

The screw compressors and screw expander isentropic part-load efficiencies are subject to volumetric and internal leakage efficiencies, as described by Eppinger et al. [30] (Equation (43)):

$$\eta_{is_pl} = \eta_{is_fl} \cdot \left(\frac{\eta_{v_pl}}{\eta_{v_fl}}\right) \cdot \left(\frac{\eta_{n_pl}}{\eta_{n_fl}}\right) \tag{43}$$

where the subscript $v$ indicates the volumetric efficiencies while the subscript $n$ stands for the leakage efficiencies.

The full-load and part-load volumetric efficiency, $\eta_v$, is described by Liu et al. [38] as shown by Equation (44):

$$\eta_v = 0.95 - 0.0125 \cdot \beta \tag{44}$$

where $\beta$ is the pressure ratio between condenser and evaporation pressure for the HP, and vice-versa for the ORC.

About the internal leakage efficiencies, they can be obtained from the following Equation (45) from Eppinger et al. [30]:

$$\eta_{n_pl} = \eta_{n_fl} \cdot f(\alpha) \tag{45}$$

where $f(\alpha)$ is a correction factor given by Liu et al. [38] as in Equation (46):

$$f(\alpha) = 0.00294 \cdot \alpha + 0.706 \tag{46}$$

Further, Liu has proposed a linear relation between volumetric and leakage efficiencies at full load, through the following Equation (47):

$$\eta_{n_fl} = a \cdot \eta_{v_fl} + b \tag{47}$$

where the linear coefficients $a$ and $b$ can be obtained thanks to a regression by interpolating two values of $\eta_{v_fl}$ at different pressure ratios. In this work, these two coefficients are

- $a = 0.893768$
- $b = 0$

for both HP compressors and the ORC expander.

### *4.2. Heat Exchanger Part-Load Operation*

During the *in-design* process, some attempts have been carried out with the aim to lower down the pinch-points and the approach-point temperature differences, in order to reduce as much as possible the heat transfer losses in the HEX. Thus, in the *off-design* model, some of these difference values have been increased to allow the part-load factor $\alpha$ to be as low as possible (see Table 12).

**Table 12.** Pinch-points and approach-point values used in the models at par-load.

| Scenario | $\Delta T_{pp_ev_hp}$ [1] | $\Delta T_{pp_cond_hp}$ [1] | $\Delta T_{pp_ev_orc}$ [1] | $\Delta T_{pp_cond_orc}$ [1] | $\Delta T_{app_eco_orc}$ [1] |
|---|---|---|---|---|---|
| 1 and 2 | 2 | 4 | 3 | 2 | 6 |

[1] All the temperature differences are in degrees Celsius.

Once the *in-design* model has been finished, the HEX areas of both HP and ORC are computed, and the values of all the areas obtained are kept constant while the part-load *off-design* model is running.

The HP condenser and intermediate pressures, as well as the ORC evaporation pressure, are kept constant by pressure switches mounted at the throttling valve inlets for the HP (points 9 and 12 in Figure 10) and at the pump outlet for the ORC (point 22 in Figure 11). The HP evaporation temperature and the ORC condensation temperature are

supposed to be kept constant by two thermostatic valves mounted at the HP evaporator outlet (point 1 in Figure 10) and at the ORC pump inlet (point 21 in Figure 11), respectively. As for the *in-design* model, all the pressure drops for both the cycles have been neglected in the *off-design* model [30].

## 5. Results and Discussion

The CB round-trip efficiency has been obtained by varying the part-load factor $\alpha$ in the part-load model. Figure 14 shows the ORC efficiency and the 2sHP COP for case studies one (Figure 14a) and two (Figure 14b), respectively, in which the fluids considered are toluene, isopentane, R1336mzz(Z), and R1233zd(E). Further, Table 13 and Figure 15 report the round-trip efficiencies for the two scenarios at part-load operation.

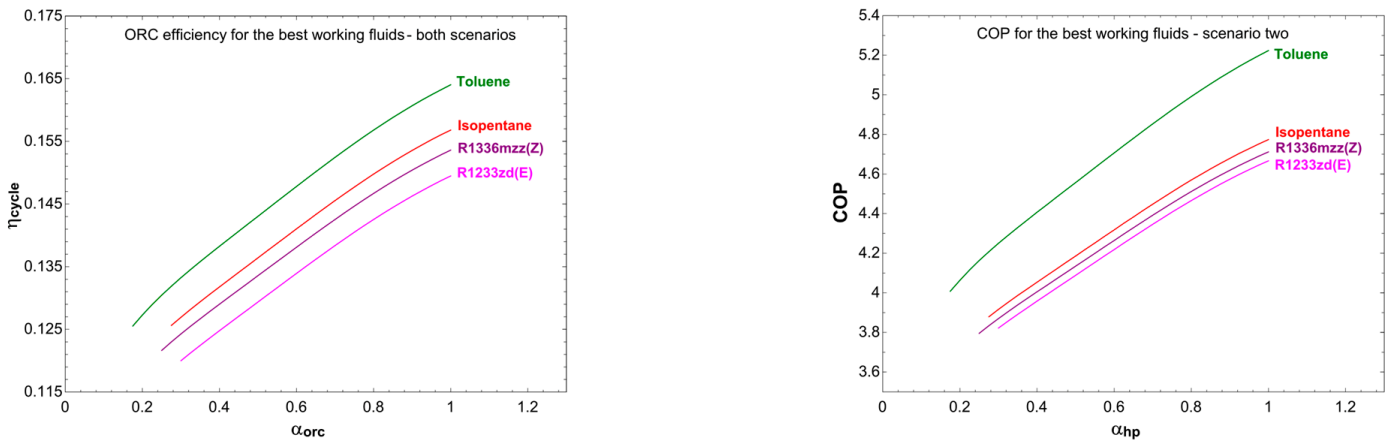


(**a**) (**b**)

**Figure 14.** The performance of the four best working fluids for both scenarios: (**a**) about the ORC; (**b**) about the 2sHP.

**Table 13.** Round-trip efficiency values obtained for maximum and minimum values of the part-load factor $\alpha$.

| Scenario | Fluid | $\alpha$ | HP COP | ORC $\eta_{cycle}$ | $\eta_{loop}$ |
|---|---|---|---|---|---|
| 1 | Toluene | 1<br>0.175 * | 2.248<br>1.834 | 0.164<br>0.125 | 0.369<br>0.230 |
| 1 | Isopentane | 1<br>0.275 * | 2.012<br>1.750 | 0.157<br>0.126 | 0.315<br>0.212 |
| 1 | R1336mzz(Z) | 1<br>0.25 * | 1.955<br>1.698 | 0.154<br>0.122 | 0.300<br>0.206 |
| 1 | R1233zd(E) | 1<br>0.3 * | 2.009<br>1.750 | 0.149<br>0.120 | 0.300<br>0.210 |
| 2 | Toluene | 1<br>0.175 * | 5.223<br>4.008 | 0.164<br>0.125 | 0.857<br>0.503 |
| 2 | Isopentane | 1<br>0.275 * | 4.774<br>3.879 | 0.157<br>0.126 | 0.748<br>0.487 |
| 2 | R1336mzz(Z) | 1<br>0.25 * | 4.712<br>3.795 | 0.154<br>0.122 | 0.724<br>0.462 |
| 2 | R1233zd(E) | 1<br>0.3 * | 4.666<br>3.822 | 0.149<br>0.120 | 0.697<br>0.459 |

* Last working value of the part-load factor $\alpha$.

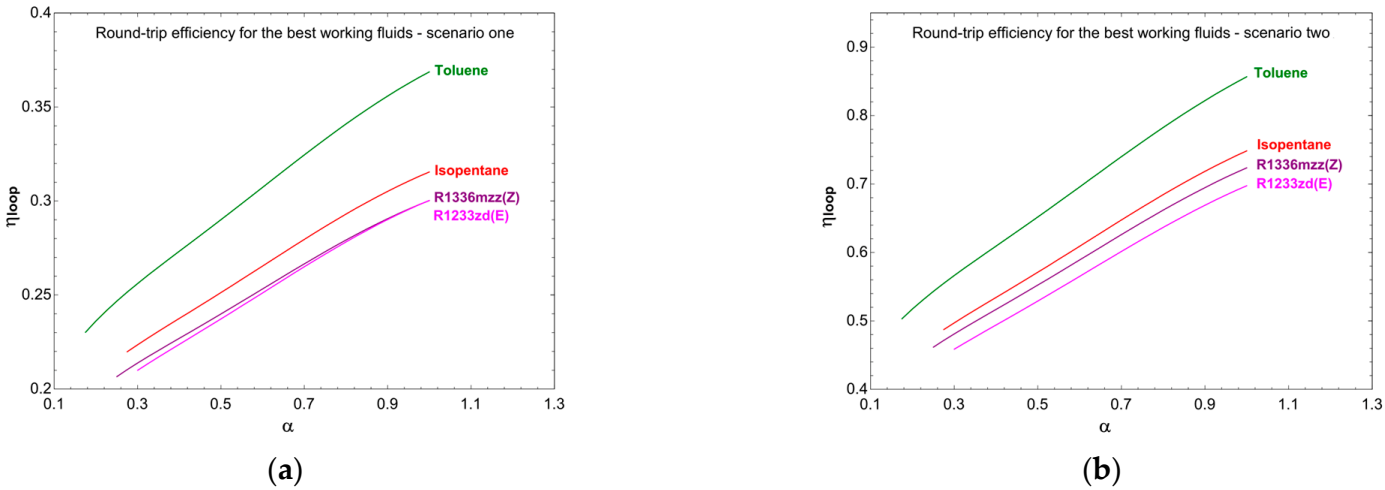


**Figure 15.** The round-trip efficiencies of the four best working fluids: (**a**) about the first scenarios; (**b**) about scenario two B.

As can be inferred from Figure 14, the best ORC and 2sHP performances are those relative to toluene and isopentane. As stated at the end of Section 2.1, since toluene has a very low saturation pressure at the ORC condenser and 2sHP evaporator working temperatures, and since isopentane has a low flash point, they must be discarded for case one. The working temperatures of the 2sHP in scenario two, instead, allow the use of toluene, the best-performing fluid in Figure 14b. Further, R1336mzz(Z) is better performing with respect to R1233zd(E), so it has been chosen as a working fluid for the ORC in both case studies one and two. Nevertheless, for what concerns the ORC, both R1336mzz(Z) and R1233zd(E) are good choices as working fluid.

### *5.1. The Round-Trip Efficiency of the Carnot Battery*

In Figure 15, it is possible to observe the round-trip efficiencies obtained for cases one and two, where both the 2sHP and the ORC use the same working fluid. It is worth noting that, while in scenario two there is still a performance advantage about R1366mzz(Z), in the first case, R1366mzz(Z) and R1233zd(E) could be considered as having equivalent performances from an energy efficiency point of view.

In Table 13 are reported some round-trip efficiency values calculated at full and at the minimum part-load obtainable with the pinch-point temperature differences adopted. With the pinch-point values as in Table 12, the simulations have stopped at different part-load factor $\alpha$, based on the kind of fluid adopted, and it has not been possible to perform the simulations until the part-load factor reached the value of $\alpha$ = 0.1. R1336mzz(Z) has been selected as the working fluid for both machines in the first scenario and for ORC in the second, since it has a slightly better performance in the off-design operation, while, if a higher minimum pressure in both cycles were preferred, then R1233zd(E) would be chosen (see Figure 9 for the fluids saturation pressures).

Table 14 shows the performances obtained about the two scenarios considered with the selected working fluids. In scenario one, R1336mzz(Z) has been used for both the ORC and 2sHP, while in scenario two, toluene has been adopted for the 2sHP, keeping R1336mzz(Z) for the ORC.

At full load, the round-trip efficiency of the CB for case two resulted to be about $\eta_{Loop}$ = 0.80. The simulation performed with the same temperatures and pinch-point temperature differences, using the R1336mzz(Z) instead of toluene as the working fluid in the 2sHP, shows that the round-trip efficiency at full load resulted to be about $\eta_{Loop}$ = 0.72, a lower value with respect to the case with toluene, consistent with the preliminary analysis.

**Table 14.** Some round-trip efficiency values obtained about the final part-load analysis.

| Scenario | $\alpha$ | HP COP | ORC $\eta_{cycle}$ | $\eta_{loop}$ |
|---|---|---|---|---|
| 1 | 1 | 1.955 | 0.154 | 0.300 |
| | 0.25 * | 1.698 | 0.122 | 0.206 |
| 2 | 1 | 5.223 | 0.154 | 0.802 |
| | 0.25 * | 4.162 | 0.122 | 0.506 |

* Last working value of the part-load factor $\alpha$.

After some research in the literature on the several works concerning the CB, we have found that very few of them [18–21,30,39] are in some way comparable with our work and are reported in Table 15, because the vast majority consider very different temperature ranges and working fluid types. Moreover, the comparable works have different hypotheses on the kind of the machines, on the heat exchangers, and the pinch-points, considering just the design situation, and thus resulting in a round-trip efficiency values dispersion.

**Table 15.** Some CB round-trip efficiency values from other authors found in the literature.

| Authors | Fluids | Maximum Temp [°C] | Minimum Temp [°C] | Intermediate Temp [°C] | Scenario | Round-Trip Efficiency |
|---|---|---|---|---|---|---|
| Eppinger et al. [30] | R1233zd(E) | 120 | 30 | 75 | 2 | 0.52 |
| Frate et al. [19] | R1233zd(E) | 130 | 35 | 80 | 2 | 0.75 |
| Fan et al. [39] | R1336mzz(Z) | 130 | 35 | - | 1 | 0.27 |
| Frate et al. [19] | Toluene | 130 | 35 | 80 | 2 | 0.58 |
| Dumont et al. [18] | R1233zd(E) | 78 | 20 | 75 | 2 | 0.82 |
| Frate et al. [21] | R1233zd(E) | 100–170 | 17 | 75 | 2 | 1.02 |
| Frate et al. [21] | R1336mzz(Z) | 100–170 | 17 | 75 | 2 | 1.03 |

Frate et al. [19] have reported a CB round-trip efficiency about several working fluids for a device operating between similar temperature ranges if compared with those of the present work, for a case analogous to our second scenario. Our model, with the aim to verify the consistency of the performance parameters at full-load in-*design* conditions, has then been run with the data from Frate et al. [19,20] for some working fluids, considering a single-stage HP, for round-trip efficiency comparison. The ORC condenser temperature has been set at 35 °C, and a storage efficiency $\eta_{Storage}$ = 0.9 has been introduced, as in Frate's work. Results are reported in the following Table 16, where the results for the CB with a 2sHP and an ORC condenser temperature of 17 °C are also shown.

**Table 16.** A comparison between the CB round-trip efficiency for several fluids from Frate et al. [19] and those ones calculated with our model with the data from Frate et al. [19] and the present work considering the storage efficiency $\eta_{Storage}$ = 0.9.

| Fluid | Paper | DHN Storage Temp [°C] | PCM Storage Temp [°C] | ORC Condenser Temp [°C] | HP Stages | Round-Trip Efficiency | Delta |
|---|---|---|---|---|---|---|---|
| Toluene | Frate et al. [19] | 80 | 120 | 35 | 1 | 0.58 | −0.05 |
| | Present work | 80 | 121 | 35 | 1 | 0.53 | |
| | Present work | 80 | 121 | 17 | 2 | 0.77 | |
| R1233zd(E) | Frate et al. [19] | 80 | 120 | 35 | 1 | 0.41 | +0.02 |
| | Present work | 80 | 121 | 35 | 1 | 0.43 | |
| | Present work | 80 | 121 | 17 | 2 | 0.63 | |
| n-Pentane | Frate et al. [19] | 80 | 120 | 35 | 1 | 0.44 | +0.04 |
| | Present work | 80 | 121 | 35 | 1 | 0.48 | |
| | Present work | 80 | 121 | 17 | 2 | 0.69 | |

**Table 16.** *Cont.*

| Fluid | Paper | DHN Storage Temp [°C] | PCM Storage Temp [°C] | ORC Condenser Temp [°C] | HP Stages | Round-Trip Efficiency | Delta |
|---|---|---|---|---|---|---|---|
| Isopentane | Frate et al. [19] | 80 | 120 | 35 | 1 | 0.41 | +0.06 |
| | Present work | 80 | 121 | 35 | 1 | 0.47 | |
| | Present work | 80 | 121 | 17 | 2 | 0.67 | |
| R245fa | Frate et al. [19] | 80 | 120 | 35 | 1 | 0.37 | +0.04 |
| | Present work | 80 | 121 | 35 | 1 | 0.41 | |
| | Present work | 80 | 121 | 17 | 2 | 0.59 | |
| Isobutane | Frate et al. [19] | 80 | 120 | 35 | 1 | 0.28 | +0.04 |
| | Present work | 80 | 121 | 35 | 1 | 0.32 | |
| | Present work | 80 | 121 | 17 | 2 | 0.46 | |
| Cyclopentane | Frate et al. [19] | 80 | 120 | 35 | 1 | 0.52 | +0.00 |
| | Present work | 80 | 121 | 35 | 1 | 0.52 | |
| | Present work | 80 | 121 | 17 | 2 | 0.73 | |
| Benzene | Frate et al. [19] | 80 | 120 | 35 | 1 | 0.56 | −0.04 |
| | Present work | 80 | 121 | 35 | 1 | 0.52 | |
| | Present work | 80 | 121 | 17 | 2 | 0.75 | |
| Cyclohexane | Frate et al. [19] | 80 | 120 | 35 | 1 | 0.52 | +0.01 |
| | Present work | 80 | 121 | 35 | 1 | 0.53 | |
| | Present work | 80 | 121 | 17 | 2 | 0.76 | |

Taking a look at Table 16, it is worth noting that, adopting the same temperatures and the same HP configuration, the difference in the round-trip efficiency is between zero and 0.06. This difference can be due to different hypothesis about pinch-points, undercooling or superheating of the working fluid, and the control system strategy.

Figure 16a,b shows the 2sHP characteristic curves obtained about the two studied scenarios, while Figure 17 shows the ORC characteristic curve for both the case studies.

As can be noted from Figures 16 and 17 and Table 14, despite the efforts to keep the cycle constant to preserve the CB round-trip efficiency values, as much as possible, near to the nominal ones, they noticeably decrease within the part-load operation.

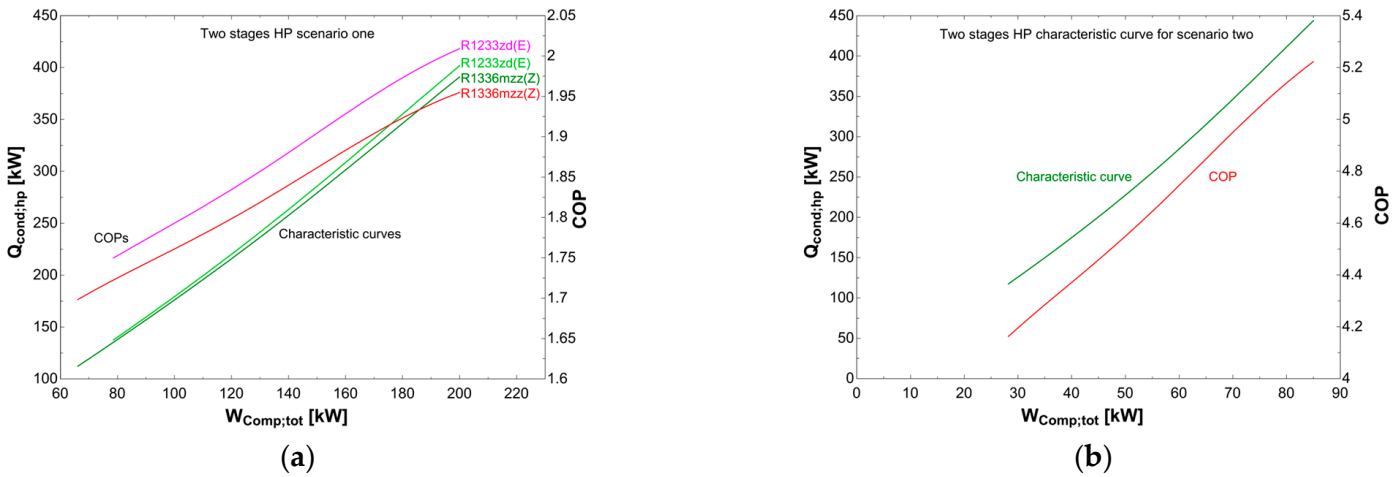


**Figure 16.** The two-stage HP characteristic curves: (**a**) about the first scenario for R1336mzz(Z) and R1233zd(E); (**b**) about the second scenario for toluene. Characteristic curves are in green, COPs in red and fuchsia.

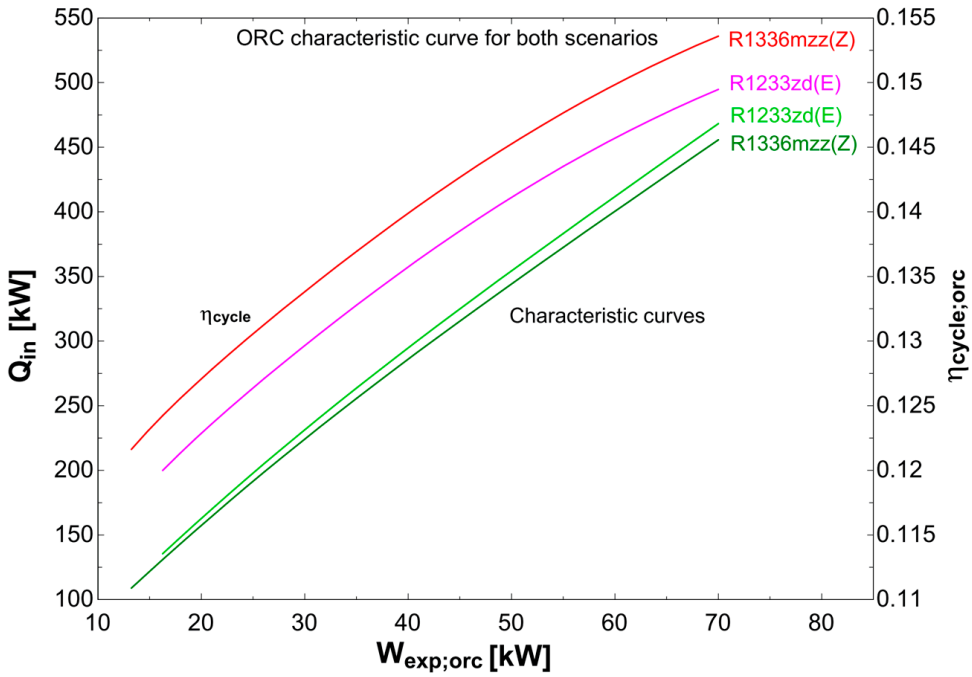


**Figure 17.** The ORC characteristic curve for both scenarios with R1336mzz(Z) and R1233zd(E) as the working fluid. Characteristic curves are in green, COPs in red and fuchsia.

This highlights the importance of choosing the right HP size, and thus the CB one, to satisfy the users' needs, because otherwise the whole device would work at part-load with a lower round-trip efficiency. Also, from Figure 16a, it can be noted that the characteristic curves for the two working fluids are very close. In addition, all characteristic curves of both HP and ORC are very close to linear relations, making the utilization of the results of this study in a MILP optimization procedure easier.

### *5.2. Conclusions and Perspectives*

After a preliminary analysis of many working fluids, a couple of them have been chosen to be used in a two-stage HP and an ORC constituting a CB. Two scenarios have been taken into account. The first one considers the ground at a constant temperature of 12 °C as a heat thermal storage (CStor) that exchanges heat with the HP evaporator and the ORC condenser, while the HP condenser and the ORC evaporator exchange heat with a latent heat HTHStor at 121 °C. A second scenario, instead, considers the HP taking heat from a sensible heat thermal storage (TStor), connected with the DHN of an EC. In this second case, the heat received by the HP condenser is at 80 °C, while the ORC and the HTHStor operate as in the first case.

The analysis results shows that toluene is always the best-performing fluid, but it can be used only in the second scenario because of the too low saturation pressure;

The working fluid selected for the first scenario has been R1336mzz(Z) for both HP and ORC. In the second case, toluene has been considered as the working fluid of the HP, while no changes have been introduced for the ORC. At the nominal operations, the total electric energy amount absorbed by the two HP compressors has been 200 kW in the first scenario and 85 kW in the second. The electric energy output of the ORC has been considered to be 70 kW for both cases.

The development of an *in-design* CB model allowed computing of the areas of the HEXs, depending on the chosen pinch-points and approach-point temperature differences, so that a following CB *off-design* model has been obtained to perform a part-load analysis of the behavior of the CB itself. Thus, the round-trip efficiency values and the machine's characteristic curves have been calculated, based on the variation of the part-load factor $\alpha$.

As can be inferred from the results of the two scenarios considered, we can conclude that:

- The round-trip efficiencies of a CB realized as in the case one has to be regarded as too poor (even if toluene were used the round-trip efficiency would not be greater than 0.37).
- A CB, as in case two, could be a good device in order to store and release energy when desired. In fact, a design round-trip efficiency of about 80% is a high value, justifying the hypothesis of performance in line with the better thermo-mechanical energy storages also for the real device, where some penalization is expected because of pressure losses.
- The round-trip efficiencies depend on the part-load operation so that a proper optimal choice of the CB size appears mandatory for taking advantage of the good design round-trip efficiency values.
- When the minimum temperature of the HP evaporator is greater than about 65 °C, toluene shows acceptable saturation pressure, so it can be used in order to obtain a better HP COP.
- When the minimum temperature of the HP evaporator or of the ORC condenser is low (in the cases considered 7 °C and 15 °C, respectively), toluene cannot be adopted because of its too low saturation pressure. In this case, both R1233zd(E) and R1336mzz(Z) seem to be good. So, R1336mzz(Z) could be preferred because it has a slightly better performance in the off-design operation, while, if a higher minimum pressure in both cycles were needed, then R1233zd(E) could be the proper choice.

The possible benefits of implementing a CB into the EC, to reduce part of the energy dependency from the grid, will be studied in future work. The results of this study show that the HP and the ORC characteristic curves are close to linear relations, so that they could be linearized and used in a MILP thermo-economic optimization model of the EC [3]. Further, a characteristic curves family could be developed through a study of the CB size variation to obtain a response surface, which could be exploited to get the CB optimal size for the EC considered.

**Author Contributions:** Conceptualization, M.C. and M.R.; Methodology, E.N. and M.R.; Software, E.N.; Validation, R.D.S. and M.C.; Formal analysis, R.D.S. and M.R.; Investigation, E.N., M.C. and M.R.; Resources, M.C. and M.R.; Data curation, E.N., R.D.S. and M.R.; Writing—original draft, E.N. and R.D.S.; Writing—review & editing, E.N. and R.D.S.; Visualization, E.N., R.D.S., M.C. and M.R.; Supervision, M.C. and M.R. All authors have read and agreed to the published version of the manuscript.

**Funding:** This research received no external funding.

**Data Availability Statement:** All the new data obtained by this study are presented in the paper.

**Conflicts of Interest:** The authors declare no conflict of interest.

## Nomenclature

| | |
|---|---|
| 2sHP | Two-stages heat pump |
| a | Slope of a straight line |
| b | Intercept of a straight line |
| $C_1$ | HEX geometrical factor |
| CB | Carnot Battery |
| COP | Coefficient of performance |
| $C_{p,v}$ | Specific heat at constant pressure of the vapor fluid phase, kJ/kg K |
| CStor | Cold thermal energy storage |
| $D_b$ | Tube bundle diameter, m |
| DHN | District Heating Network |
| $d_i$ | Inner tube diameter, m |
| $d_o$ | Outer tube diameter, m |
| DS | Energy Community Distribution Substation |
| EC | Energy Community |
| Fb | Factor for the calculation of the convective heat transfer coefficient on the evaporator shell side |
| $g$ | Gravity acceleration, m/s$^2$ |

| | |
|---|---|
| $h$ | Specific enthalpy, kJ/kg |
| HEX | Heat exchanger |
| HP | Heat pump |
| $h_s$ | HEX convective heat transfer coefficient on the shell side, kW/m$^2$ K |
| $h_t$ | HEX convective heat transfer coefficient on the tubes side, kW/m$^2$ K |
| HTHStor | High-temperature heat storage |
| ICE | Internal combustion engine |
| K | A HEX factor |
| $k_l$ | Thermal conductivity of the liquid fluid phase, kW/m K |
| LMTD | Logarithmic mean temperature difference, °C |
| $\dot{m}$ | Mass flow, kg/s |
| $\dot{m}_{cond}$ | HP condenser mass flow, kg/s |
| $\dot{m}_{ev}$ | HP evaporator mass flow, kg/s |
| MGT | Micro gas turbine |
| MILP | Mixed-Integer Linear Programming |
| MM | Molar mass, kg/kmol |
| $\dot{m}_{orc_pl}$ | ORC mass flow, kg/s |
| $n$ | A HEX factor |
| $N_p$ | HEX number of passages |
| $N_t$ | Number of tubes in the HEX |
| Nu | Nusselt number |
| ORC | Organic Rankine cycle |
| PCM | Phase change material |
| $P_{Cr}$ | Critical pressure, bar |
| $P_{int}$ | HP intermediate pressure, bar |
| Pr | Prandtl number |
| PR | Pressure ratio |
| $P_t$ | Pitch of the tube bundle |
| PTES | Pumped thermal energy storage |
| PVp | Photovoltaic panel |
| Q | Heat flow, kW |
| Re | Reynolds number |
| RES | Renewable energy sources |
| RE | Renewable energy |
| STP | Solar thermal panel |
| $T_{cond}$ | Condensation temperature, °C |
| $T_{ev}$ | Evaporation temperature, °C |
| TStor | Hot thermal energy storage |
| $T_w$ | Temperature of the HEX water inside the tubes, °C |
| U | Overall heat transfer coefficient, kW/m$^2$ K |
| UA | Overall conductance, kW/K |
| $W_{comp}$ | HP compressor work, kW |
| $W_{gross_exp}$ | ORC expander gross work, kW |
| $W_{net_exp}$ | ORC expander net work, kW |
| $W_{pump}$ | ORC pump work, kW |
| $\alpha$ | Part load factor |
| $\alpha_{nb}$ | Factor for the calculation of the convective heat transfer coefficient on the evaporator shell side |
| $\beta$ | Pressure ratio |
| $\Delta T$ | Temperature difference, °C |
| $\Delta T_{app}$ | Approach-point temperature difference, °C |
| $\Delta T_{pp}$ | Pinch-point temperature difference, °C |
| $\varepsilon$ | Regenerator efficacy |
| $\eta_{el}$ | Electric efficiency |
| $\eta_{is}$ | Isentropic efficiency |
| $\eta_{loop}$ | Round-trip efficiency |
| $\eta_{mec}$ | Mechanical efficiency |
| $\eta_n$ | Leakage efficiency |

| | |
|---|---|
| $\eta_{orc}$ | ORC efficiency |
| $\eta_{storage}$ | Thermal storage efficiency |
| $\eta_v$ | Volumetric efficiency |
| $\lambda$ | Latent heat of condensation, kJ/kg |
| $\lambda'$ | Modified latent heat of condensation, $\lambda' = \lambda + C_{P,V} \cdot (T_V - T_{sat})$, kJ/kg |
| $\mu_l$ | Dynamic viscosity of the liquid fluid phase, N/m$^2$ s |
| $\rho_l$ | Density of the liquid fluid phase, kg/m$^3$ |
| $\rho_v$ | Density of the vapor fluid phase, kg/m$^3$ |

## References


1. International Energy Agency (IEA). Evolution of Key Regional Natural Gas Prices, June 2021–October 2022. Available online: https://www.iea.org/data-and-statistics/charts/evolution-of-key-regional-natural-gasprices-june-2021-october-2022 (accessed on 15 February 2023).
2. International Energy Agency (IEA). Evolution of Energy Prices, October 2020–January 2022. Available online: https://www.iea.org/data-and-statistics/charts/evolution-of-energy-prices-oct-2020-jan-2022 (accessed on 15 February 2023).
3. International Energy Agency (IEA). Evolution of Energy Prices, 2020–2021. Available online: https://www.iea.org/data-and-statistics/charts/evolution-of-energy-prices-2020-2021 (accessed on 17 February 2023).
4. International Energy Agency (IEA). How to Avoid Gas Shortages in the European Union in 2023. Available online: https://www.iea.org/reports/how-to-avoid-gas-shortages-in-the-european-union-in-2023 (accessed on 17 February 2023).
5. De Souza, R.; Casisi, M.; Micheli, D.; Reini, M. A Review of Small–Medium Combined Heat and Power (CHP) Technologies and Their Role within the 100% Renewable Energy Systems Scenario. *Energies* **2021**, *14*, 5338. [CrossRef]
6. International Energy Agency (IEA). Grid-Scale Storage, Paris. Available online: https://www.iea.org/reports/grid-scale-storage, (accessed on 4 April 2023).
7. Sadr, A.N.; Shekaramiz, M.; Zarinfar, M.; Esmaily, A.; Khoshtarash, H.; Toghraie, D. Simulation of mixed-convection of water and nano-encapsulated phase change material inside a square cavity with a rotating hot cylinder. *J. Energy Storage* **2022**, *47*, 103606. [CrossRef]
8. Miansari, M.; Nazari, M.; Toghraie, D.; Akbari, O.A. Investigating the thermal energy storage inside a double-wall tank utilizing phase-change materials (PCMs). *J. Therm. Anal. Calorim.* **2020**, *139*, 2283–2294. [CrossRef]
9. Yan, S.-R.; Fazilati, M.A.; Samani, N.; Ghasemi, H.R.; Toghraie, D.; Nguyen, Q.; Karimipour, A. Energy efficiency optimization of the waste heat recovery system with embedded phase change materials in greenhouses: A thermo-economic-environmental study. *J. Energy Storage* **2020**, *30*, 101445. [CrossRef]
10. Katsaprakakis, D.A.; Dakanali, I.; Condaxakis, C.; Christakis, D.G. Comparing electricity storage technologies for small insular grids. *Appl. Energy* **2019**, *251*, 113332. [CrossRef]
11. Abdon, A.; Zhang, X.; Parra, D.; Patel, M.K.; Bauer, C.; Worlitschek, J. Techno-economic and environmental assessment of stationary electricity storage technologies for different time scales. *Energy* **2017**, *139*, 1173–1187. [CrossRef]
12. Chatzivasileiadi, A.; Ampatzi, E.; Knight, I. Characteristics of electrical energy storage technologies and their applications in buildings. *Renew. Sustain. Energy Rev.* **2013**, *25*, 814–830. [CrossRef]
13. Benato, A.; Stoppato, A. Pumped Thermal Electricity Storage: A technology overview. *Therm. Sci. Eng. Prog.* **2018**, *6*, 301–315. [CrossRef]
14. Steinmann, W.-D. Thermo-mechanical concepts for bulk energy storage. *Renew. Sustain. Energy Rev.* **2017**, *75*, 205–219. [CrossRef]
15. Gautam, K.R.; Andresen, G.B.; Victoria, M. Review and Techno-Economic Analysis of Emerging Thermo-Mechanical Energy Storage Technologies. *Energies* **2022**, *15*, 6328. [CrossRef]
16. Steinmann, W.-D.; Jockenhöfer, H.; Bauer, D. Thermodynamic Analysis of High-Temperature Carnot Battery Concepts. *Energy Technol.* **2019**, *8*, 1900895. [CrossRef]
17. Casisi, M.; Pinamonti, P.; Reini, M. Increasing the Energy Efficiency of an Internal Combustion Engine for Ship Propulsion with Bottom ORCs. *Appl. Sci.* **2020**, *10*, 6919. [CrossRef]
18. Dumont, O.; Lemort, V. Mapping of performance of pumped thermal energy storage (Carnot battery) using waste heat recovery. *Energy* **2020**, *211*, 118963. [CrossRef]
19. Frate, G.F.; Ferrari, L.; Desideri, U. Rankine Carnot Batteries with the Integration of Thermal Energy Sources: A Review. *Energies* **2020**, *13*, 4766. [CrossRef]
20. Frate, G.F.; Antonelli, M.; Desideri, U. A novel Pumped Thermal Electricity Storage (PTES) system with thermal integration. *Appl. Therm. Eng.* **2017**, *121*, 1051–1058. [CrossRef]
21. Frate, G.F.; Ferrari, L.; Desideri, U. Multi-criteria investigation of a pumped thermal electricity storage (PTES) system with thermal integration and sensible heat storage. *Energy Convers. Manag.* **2020**, *208*, 112530. [CrossRef]
22. Dumont, O.; Frate, G.F.; Pillai, A.; Lecompte, S.; De Paepe, M.; Lemort, V. Carnot battery technology: A state-of-the-art review. *J. Energy Storage* **2020**, *32*, 101756. [CrossRef]
23. Energy Storage Task 36—Carnot Batteries. Available online: https://www.eces-a36.org/index.php/about-annex-36/ (accessed on 6 April 2023).

24. De Souza, R.; Nadalon, E.; Casisi, M.; Reini, M. Optimal Sharing Electricity and Thermal Energy Integration for an Energy Community in the Perspective of 100% RES Scenario. *Sustainability* **2022**, *14*, 10125. [CrossRef]
25. Casisi, M.; Buoro, D.; Pinamonti, P.; Reini, M. A Comparison of Different District Integration for a Distributed Generation System for Heating and Cooling in an Urban Area. *Appl. Sci.* **2019**, *9*, 3521. [CrossRef]
26. Casisi, M.; Costanzo, S.; Pinamonti, P.; Reini, M. Two-Level Evolutionary Multi-objective Optimization of a District Heating System with Distributed Cogeneration. *Energies* **2019**, *12*, 114. [CrossRef]
27. Casisi, M.; De Nardi, A.; Pinamonti, P.; Reini, M. Effect of different economic support policies on the optimal synthesis and operation of a distributed energy supply system with renewable energy sources for an industrial area. *Energy Convers. Manag.* **2015**, *95*, 131–139. [CrossRef]
28. Vecchi, A.; Sciacovelli, A. Thermo-mechanical energy storage options for long-duration storage—A techno-economic comparative assessment of established and novel concepts. In Proceedings of the ECOS, Copenhagen, Denmark, 3–7 July 2022.
29. Available online: https://fchartsoftware.com/ees/ (accessed on 6 April 2023).
30. Eppinger, B.; Muradi, M.; Scharrer, D.; Zigan, L.; Bazan, P.; German, R.; Will, S. Simulation of the Part Load Behavior of Combined Heat Pump-Organic Rankine Cycle Systems. *Energies* **2021**, *14*, 3870. [CrossRef]
31. Available online: http://www.triogen.nl/technology/what-is-an-orc (accessed on 6 April 2023).
32. Mohamed, S.A.; Al-Sulaiman, F.A.; Ibrahim, N.I.; Zahir, H.; Al-Ahmed, A.; Saidur, R.; Yılbaş, B.S.; Sahin, A.Z. A review on current status and challenges of inorganic phase change materials for thermal energy storage systems. *Renew. Sustain. Energy Rev.* **2017**, *70*, 1072–1089. [CrossRef]
33. Ge, H.; Li, H.; Mei, S.; Liu, J. Low melting point liquid metal as a new class of phase change material: An emerging frontier in energy area. *Renew. Sustain. Energy Rev.* **2013**, *21*, 331–346. [CrossRef]
34. Farid, M.M.; Khudhair, A.M.; Razack, S.A.K.; Al-Hallaj, S. A review on phase change energy storage: Materials and applications. *Energy Convers. Manag.* **2004**, *45*, 1597–1615. [CrossRef]
35. Nitsche, M.; Gbadamosi, R. *Heat Exchanger Design Guide—A Practical Guide for Planning, Selecting and Designing of Shell and Tube Exchangers*; Elsevier: Amsterdam, The Netherlands, 2016. [CrossRef]
36. Serth, R.W.; Lestina, T.G. *Process Heat Transfer—Principles, Applications and Rules of Thumb*, 2nd ed.; Elsevier: San Diego, CA, USA, 2014. [CrossRef]
37. Mazzi, N.; Rech, S.; Lazzaretto, A. Off-design dynamic model of a real Organic Rankine Cycle system fuelled by exhaust gases from industrial processes. *Energy* **2015**, *90*, 537–551. [CrossRef]
38. Liu, J.; Li, Q.; Wang, F.; Zhou, L. A new model of screw compressor for refrigeration system simulation. *Int. J. Refrig.* **2012**, *35*, 861–870. [CrossRef]
39. Fan, R.; Xi, H. Exergoeconomic optimization and working fluid comparison of low-temperature Carnot battery systems for energy storage. *J. Energy Storage* **2022**, *51*, 104453. [CrossRef]


**Disclaimer/Publisher's Note:** The statements, opinions and data contained in all publications are solely those of the individual author(s) and contributor(s) and not of MDPI and/or the editor(s). MDPI and/or the editor(s) disclaim responsibility for any injury to people or property resulting from any ideas, methods, instructions or products referred to in the content.